Universiteit Utrecht

Faculty of Science

Jet characterisation of W bosons in pp collisions at $\sqrt{s_{NN}} = 5.02$ TeV

Bachelor Thesis Physics & Astronomy

Elias F. Dubbeldam

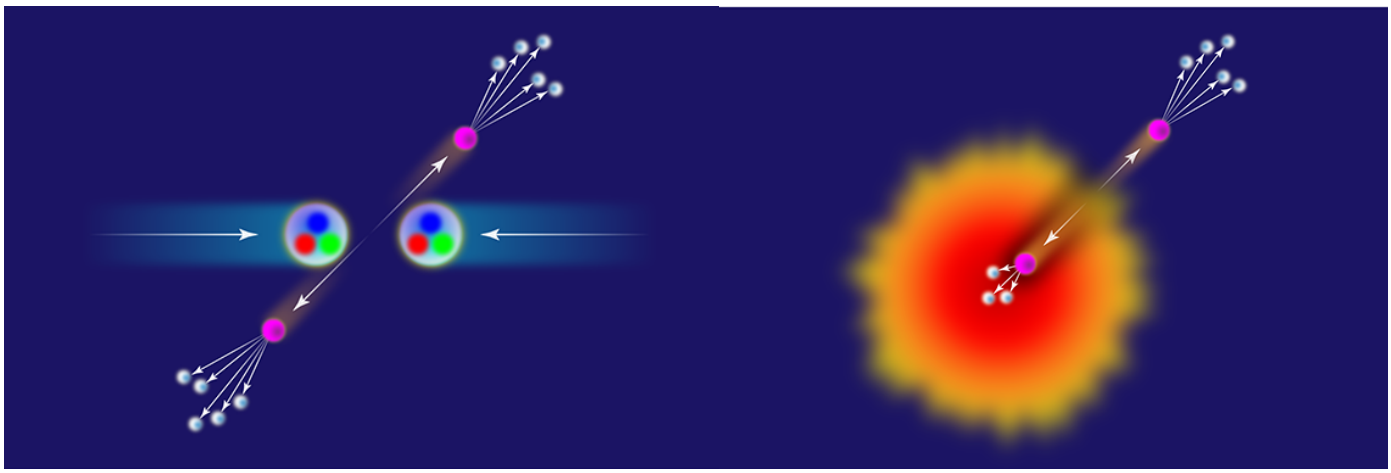

Supervisor:

Dr. Marta Verweij
Institute for Subatomic Physics

June, 2019

Abstract

The Quark–Gluon Plasma (QGP), created in high-energy nuclear collisions, can be studied by measuring the remnants of the hard scattered particles. They decay in jets, collimated sprays of particles, which lose energy to the QGP by jet quenching. If the collision produces a W boson, the jets originating from it start interacting at later times with the QGP. This time delay of the W boson can give information about the time evolution of the plasma. To distinguish W bosons in measurements of pp collisions, their jet characteristics are compared in PYTHIA and JEWEL. W boson signal events are compared with other W boson events that contain mixed and subsequently constituent subtracted thermal events. This comparison shows that a minimal cut on a few jet characteristics can be applied to increase the distinctiveness of W bosons. Based on these findings we establish cuts on jet characteristics that optimise the significance and increase the ratio of W bosons in measurements of pp collisions.

(Left) The partons that compose protons can hit each other when the protons are collided at high speeds. Only the quarks of the proton are depicted here in blue, red and green. The partons will fly away as hard scattering particles (pink) and will decay in jets of particles (white). The particles within the jets will be detected after they are hadronized. (Right) After the proton-proton the hard scattering particles and jets will propagate trough the Quark–Gluon Plasma (QGP). The jets can be extinguished, or *quenched* by the QGP. The effect of quenching can learn us more about the properties of the QGP. Figures retrieved from [1].

Contents

1 Introduction

Our world is made up from molecules. These molecules consist of atoms, which consist of protons and neutrons (hadrons) with electrons circling around them. The proton and neutrons are built from quarks and gluons (partons) and are together with electrons part of Standard Model (SM). The SM describes all the elementary particles where matter and antimatter consists of. During the early universe, shortly after the Big Bang, hadrons did not exist. The universe was filled with a hot dense plasma consisting of quark and gluons, known as the *Quark–Gluon Plasma* (QGP). Quarks and gluons were roaming freely trough the QGP until the temperature and density of the universe dropped below a certain level [2]. Partons started to be confined and hadrons are formed.

From studying the QGP, we can learn about the Big Bang and the structure of our universe. To study it, protons or heavy nuclei are being collided at ultrarelativistic speeds in an accelerator, the Large Hadron Collider (LHC) [3] at CERN. During this collision, the temperature is so high that the protons or nuclei melt and the QGP is reproduced. The temperature cools down quickly, making the lifespan of the QGP too short to study it by direct measurement [4]. But during the existence, partons traverse the plasma and fragment into collimated sprays of particles, called jets.

Measurements of the remnants of the collisions in the LHC are conducted at the ALICE detector. These measurements characterise the jets. The QGP can indirectly be described by the characteristics of the jets [5]. An elementary particle forming jets that stands out when describing QGP is the W boson. Jets originating from other particles are produced simultaneously with the collision, while the jets that originate from the W bosons start interacting with the plasma at later times [6]. The quark-antiquark pair decaying from the W bosons propagate a certain distance before they start interacting independently with the medium.

To use the delay of W bosons in comparison with other particles, the W bosons need to be identified in the measurement. Because a lot of different particles are produced during a proton-proton (pp) or Pb-Pb collision, the jets originating from W are at first sight indistinguishable from the other particles. A smart selection of the measurements will help to distinguish the W bosons. This thesis will focus on the question how W bosons can be distinguished in pp collisions at $\sqrt{s_{NN}} = 5.02$ TeV by studying their jet characteristics.

The theory starts with a brief introduction about the physics of the QGP, Quantum Chromodynamics and how it is studied with the ALICE detector. Thereafter will be elaborated on jets, how they are found and characterised. The processes that produce the particles after the collision and the characterisation of these particles will be discussed. Hereupon the experimental setup is introduced. In the experimental setup will be explained which collisions are used and how the data of it is obtained in PYTHIA and JEWEL. The main part of this thesis will be the analysis of these events. Pull distributions are used to determine a suitable fit function. Jets characteristics from W bosons are studied by adding thermal events and subtracted with with the constituent striation method. The jet characteristics that are the most promising to distinguish W bosons are used to compare W bosons with dijet events. The best cuts in these jet characteristics will be determined. An optimal combination of these cuts is applied in the results. The established cuts will be applied on W boson signal

and background events from PYTHIA and compared to signal events from JEWEL. We will end with the conclusions we can draw from the results, reflecting on the performed research and suggest further research.

2 Theory

2.1 Quantum Chromodynamics

Quarks and gluons, together called partons, are elementary particles and part of the Standard Model. Quantum Chromodynamics (QCD) is the theory that describes partons and the interactions between them. Quarks are fermions and the building blocks of matter, while gluons are bosons and the force carriers. QCD has two main characteristics: *confinement* and *asymptotic freedom*.

The strength of the force of the interaction between quarks and gluons is described by the strong coupling constant [7]. The key property of the strong coupling constant is that, unlike other forces in nature, it gets less strong at shorter distances. This means that the interaction between quarks and gluons grows with increasing distance. Because of this behaviour, gluons become asymptotically free at shorter distances. They behave as quasi-free particles inside protons and neutrons.

Quarks and gluons are usually bound together and are not freely observed in nature. This phenomena is known as confinement. At increasing distances, the coupling constant becomes so strong that the gluon between the quark-antiquark pair breaks and that two quark-antiquark pairs form. It is energetically more favourable to produce a new quark-antiquark pair than increase the separation between two quarks. However, QCD predicts that quark confinement breaks down when a critical temperature or density is reached [2]. When deconfinement takes places, the QGP forms as a dense hot plasma of quarks and gluons.

2.2 ALICE

At CERN, particles are collided in the Large Hadron Collider (LHC) [3]. The LHC is the largest and most powerful particle accelerator of the world. Superconducting magnets accelerate two high energy particle beams in a 27-kilometre ring. Once the beams reach a speed very close to the speed of light (in the order of a few meter per seconds slower), the particles are collided in one of four the detectors, ATLAS, CMS, ALICE and LHCb.

ALICE (A Large ion Collider Experiment) [8, 9] is the heavy-ion detector that studies the QCD by recreating the QGP. Two Pb ions or two protons are collided at relativistic velocities. The temperature during this collision is so high that the nuclei or protons will melt and the QGP will form. The remnants of the collided particles are new formed particles which are detected by the different detectors of ALICE. ALICE has 18 individual detectors, each with a specific task. The measurements of the tracking detectors in the central barrel of ALICE are the most interesting to study W bosons. These are the Inner Tracking System (ITS) and Time Projection Chamber (TPC).

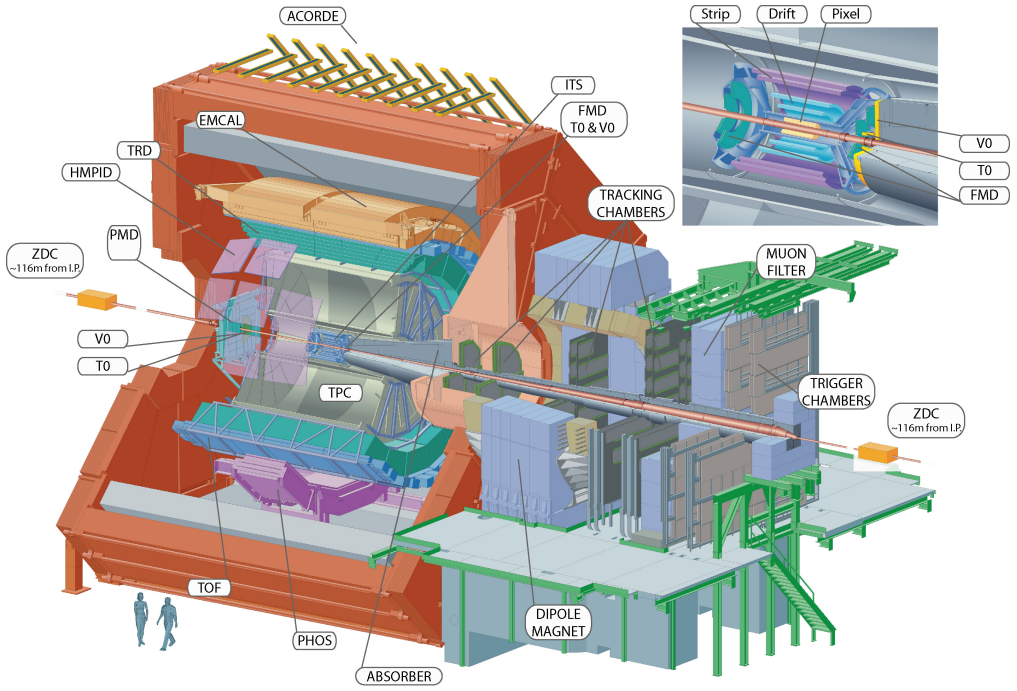

Figure 1: The ALICE detector at CERN LHC. The ITS is shown in the enlarged picture with the three layers Pixel (SPD), Drift (SDD) and Strip (SSD). Together with the TPC, which is indicated in the middle, does the ITS the tracking in the central barrel.

The ITS [10, 11] consists of three times two layers of silicon detectors. The first two layers are together the Silicon Pixel Detector (SPD), the second pair is the Silicon Drift Detector (SDD) and the last two layers form the Silicon Strip Detector (SSD). The first layer lays at $r = 3.9$ cm from the beam line and the last layer starts at $r = 43$ cm. The SPD's main focus is to determine the location of the collision and has a pseudorapidity of $|\eta| < 1.95$. The pseudorapidity is a measure for the angle between the particle and the beam and will be further explained in Section 2.5. When a charged particle passes trough one of the SDD layers, it leaves an electron behind. This electron starts to drift trough the silicon layer and is detected by one of the multiple anodes that are connected to the silicon layers. With the drift time of this electron, the y coordinate of the particle can be measured. The x coordinate is obtained from location of the anode. The SDD accepts particles with $|\eta| < 0.9$. The last pair, the SSD are important for the connection between the ITS and the next detector, the TPC. The SSD has a pseudorapidity acceptance of $|\eta| < 0.97$.

The TPC [12, 13] is the main detector for particle tracking in the central barrel. It covers the range $84.8 < r < 246.6$ cm from the beam line and has a pseudorapidity of $|\eta| < 0.9$, but higher acceptance is possible at lower momentum resolutions. The TPC is filled with $90\,\mathrm{m}^3$ gas that has more or less the same function as the silicon in the ITS. When charged particles traverse trough the TPC, they ionise the gas leaving a trail of electron behind. These electrons drift towards the end of the cylinder where they are detected and amplified by anodes.

2.3 Jets

At the LHC, two particles are accelerated at relativistic velocities. When relativistic velocities are reached, the particles are collided. The temperature during this collision is so high that the nuclei will melt and the QGP will form. The partons travel across the QGP and will interact with each other (blue stages in Figure 3) and new particles (green stages Figure 3) will be created from this interaction. The particles are accelerated in opposite direction, so the momentum in the beam axis during the collusion will be (almost) zero. This forces the newly created particles to head off back-to-back and move away from the centre of the collision. They will separately decay in constituent particles. While the created particles are moving away from the centre of the collision, the QGP is cooling down. This allows the partons to form other particles than quarks and gluons alone. The W boson is such a particle that can be created [14, 15].

The direct constituent particles from the collision, or the so called *hard scattering* particles (green stages in Figure 3), will decay in constituent particles themselves (red stages in Figure 3). These constituent particles decay again in constituent particles, and so on. All these constituent particles should conserve the momentum and energy of their *parent particle*, the particle where the constituent origins from. Because of conservation of energy, the invariant mass of the constituent particles can not be higher than that of the parent particle. Because of conversation of momentum, the constituent particles will more or less go in the same direction. Eventually, the particles will form hadrons that can be measured in the detectors of ALICE. The hadrons measured close to each other often come from the same parent particle. The constituent particles that form those hadrons are grouped as a *jet*. By measuring the hadrons one can trace back trough the jet and find characteristics of the particle that originated the jet, the hard scattering particle.

It can be hard to define which particle belongs to which jet and how many jets there are in an event. After all particles are assigned to jets, one can find the jets that originated from the same hard scattered particle. Finding the correct combination of jets is made more difficult by several processes. Important complicating processes are extra jets by hard radiating gluons and soft radiations by other interactions. Most often, the two constituent particles from the two hard scattered particles (the red stages in Figure 3) form their own distinctive jet. This means that there are are initially four jets formed when two partons interact. When quarks are formed as the constituent particles of the hard scattered particles, a quark can emit a *hard radiating gluon* that will form its own jet [16]. This means that the hard scattering particle originated three jets instead. This complicates the finding of the correct combination of jets that originated from the same hard scattered particle. When two particles are collided and interact, these two particles are not the only particles that interact. In Pb-Pb or *pp* collisions, not all partons collide and form hard scattering particles. The other particles emit *soft radiation* in the form of the decaying constituent particles that will also end up in jets [17].

When tracing back from the detected particles trough the jet to the hard scattered particle, *jet quenching* also has to be taken into account, as shown in Figure 2. Jet quenching is the modification of jets when passing trough the QGP [6]. The partons emit a *brehmstrahlung gluon* when interacting the the QGP. The emitted gluon itself will interact with the partons in the medium, resulting in a energy loss of the high momentum partons in the QGP [2, 4].

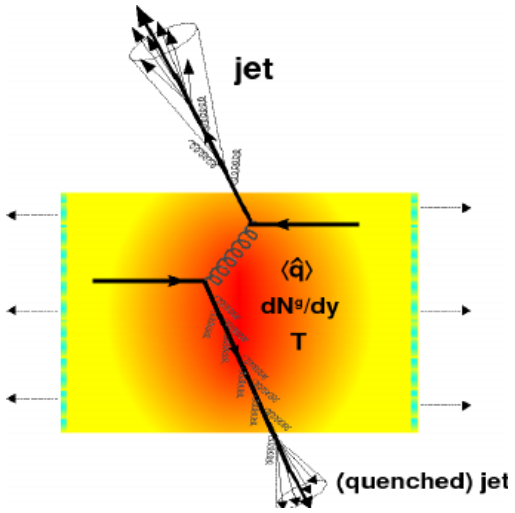

Figure 2: Jet quenching in a high energy collision between two quarks. Two hard scattering particles are formed in the the expanding QGP. The top jet moves directly out of the QGP before interacting with it. It hadronizes after radiating a few gluons outside the QGP. The bottom jet propagates trough the QGP and interacts with it by emitting brehmstrahlung gluons. The quenched jet suffers radiative energy loss and its particles will hadronize like the unquenched jet once if leaves the QGP. Figure retrieved from [18]. $\langle\hat{q}\rangle$, dN^g/dy and T can be ignored.

2.4 Production processes

In a Pb-Pb or *pp* collision, two partons can collide and form two new partons. These partons will move away from each other to conserve the momentum of the collision and decay new particle pairs. These new pairs are the constituent particles of the hard scattering particles and the start of the jets. When the hard scattering particles are only quarks or gluons, this reaction is referred as a *dijet* event [7, 15]. A few dijet event examples are $gg \to gg$, $gg \to q\bar{q}$, $qg \to qg$, $qq \to qq$, where g is a gluon and q is a quark. The example where two quarks form two new quarks is shown in Figure 3a.

A collided parton pair can also decay in other hard scattering particles than only an other parton pair. Two W bosons, a Wq or a Wg pair can also be formed as hard scattering particles [19]. The production of W bosons happens at later times than the previously discussed dijet events [6]. This delay has influence on the jet quenching effect. The differences between the dijets and W boson jet hold information about the QGP. There is about a third chance that a W boson has leptonic decay and a two third chance to decay hadronically, to a quark-antiquark pair [20]. When a W boson decays in a quark-antiquark pair, the quarks will form jets similar to the dijets originating from the dijet event. An example of a W boson production process is shown in Figure 3b.

2.5 Jet characteristics

In collider kinematics are, instead of energy and polar coordinates, *transverse momentum* p_T, *pseudo-rapidity* η, *azimuthal angle* ϕ and *mass* m used as coordinates to describe particles.

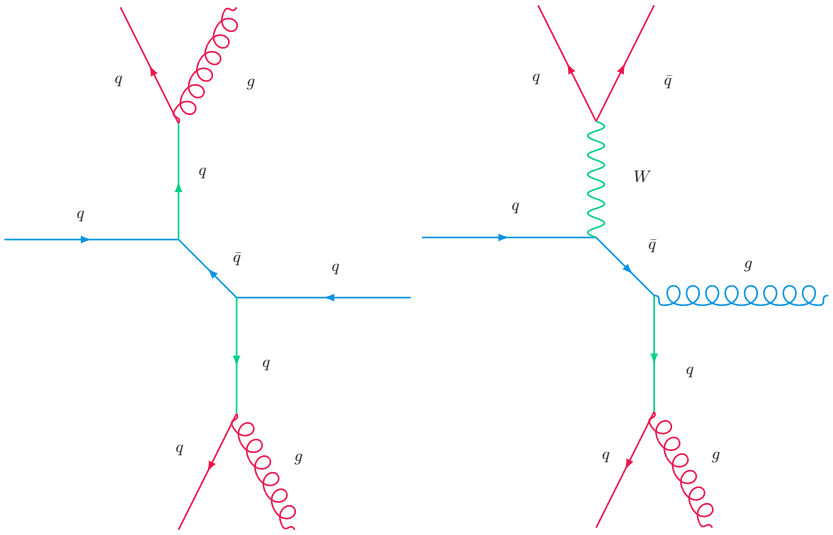

(a) Dijet event **(b)** W boson event

Figure 3: Possible production processes in pp collisions. Blue: the collided partons and the interacting particle. Green: the hard scattering particles originating directly from the collision. Red: the constituents of the hard scattering particles. They will eventually form their own distinctive jet.

If the z axis is the beam axis, p_T and ϕ are defined as the modulus and the azimuthal angle in the transverse plane, i.e.

$$p_T = \sqrt{p_x^2 + p_y^2} \tag{1}$$

and

$$\phi = \arctan\left(\frac{p_y}{p_x}\right), \tag{2}$$

as shown in Figure 4b. The polar angle θ, the angle between the particle and the beam, defines the pseudo-rapidity η, which also can be defined as the modulus of the 3-momentum:

$$\eta = -\log\left(\tan\frac{\theta}{2}\right) = \frac{1}{2}\log\left(\frac{|\vec{p}| + p_z}{|\vec{p}| - p_z}\right). \tag{3}$$

This means that if particles are going in the direction of the beam axis, $\eta = \infty$ and if the particles are moving away with a right angle of the collided particles, $\eta = 0$. Pseudo-rapidity is mainly experimentally used. Rapidity

$$y = \frac{1}{2}\log\left(\frac{E + p_z}{E - p_z}\right), \tag{4}$$

with E the energy of the jet, is mainly theoretically [21] used. With the rapidity y and the azimuthal angle ϕ, the angle between two particles is described by

$$\Delta R_{ij} = \sqrt{\Delta y_{ij}^2 + \Delta\phi_{ij}^2}, \tag{5}$$

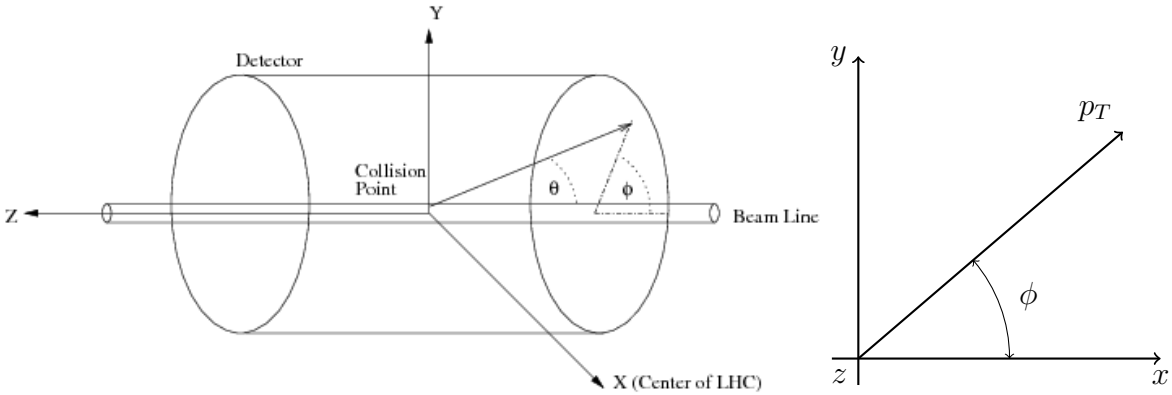

(a) Complete detector with the beam line across the z axis. Figure retrieved from [19].

(b) The $x - y$ plane in a detector, which is perpendicular to the beam axis z.

Figure 4: Schematic overview of coordinates in a collider detector.

where i, j are two particles. All these coordinates discussed so far, can be measured in a detector as shown in Figure 4a.

All measured particles will be grouped in jets by jet algorithms which will be explained in Section 2.6. The jets are described with the same coordinates p_T, η, ϕ, and m. The substructure of the jets is described by the *generalised angularities* [21, 22]. Part of these generalised angularities is defined by

$$\lambda_\beta = \sum_{i \in \text{ jet}} z_i \left(\frac{\Delta R_{i,\text{ jet}}}{R} \right)^\beta, \tag{6}$$

where z_i is the jet transverse momentum fraction of the particles within jet i. The angle between the jet axis $\Delta R_{i,\text{jet}}$ is calculated with Equation 5 where $j = \text{jet}$, and R is the jet radius. The jet transverse momentum fraction z_i is defined as the momentum fraction of the total momentum of all the particles within a jet:

$$z_i = \frac{p_{T,i}}{\sum_{j \in \text{ jet}} p_{T,j}}. \tag{7}$$

The generalised angularities hold information about the substructure of the jet and its shape. The generalised angularities become larger when there is more radiation in a jet. Therefore they are a measure of QCD radiation around the jet axis. Often they are used as a discriminator of quark and gluon jets. The specific case $\beta = 1$ tells us something about the *width* of the jet, also referred as *girth* of *broadening*. The thrust, which is closely related to the jet mass is described by the case $\beta = 2$.

2.6 Jet algorithms

To determine which particles should be assigned to which jet, algorithms are used. There are two types of jet algorithms, cone algorithms and sequential recombination algorithms. A typical cone algorithm would be [15, 23]:

1. Pick the highest p_T particle.
2. Build a cone with of radius R, with a predefined value or R. All particles inside the cone are part of the proto-jet.
3. Repeat the previous step until the direction of the cone does not change after an iteration. Exclude all particles outside the proto-jet. The particles inside the proto-jet are the jet.
4. Repeat all the steps above until all particles are assigned to jets.

A sequential recombination algorithm would typically be [15, 24]:

1. Calculate the distance d_{ij} between all particle pairs i, j.
2. Calculate the beam distance d_{iB} all particles i to the beam B.
3. Find the smallest distance of d_{ij} and d_{iB}. If d_{ij} is the smallest, combine the particles i and j into a new particle. If d_{iB} is the smallest, call it a jet and remove is from the list.
4. Repeat all the steps above until all particles are clustered into jets.

2.7 Hard scattering characterisation

To find information about the hard scattering particles, jets are combined since the right combination of jets contains all the particles that decayed from the hard scattering particle. The first characteristics to combine are instinctively the invariant mass m_{inv} and the transverse momentum $p_{T,\text{comb}}$ of the hard scattered particles. The mass m of a jet is total mass of all the hadrons within that jet. By calculating the invariant mass of two jets, the invariant mass of the hard scattered particles can be found. By combining the transverse momenta $p_{T,\text{jet}}$ of two jets, the transverse momentum of the hard scattered particle, is found. While making these combinations the coordinates that describe the jets are used. A distinction can be made between the values of these jet coordinates with *leading* and *subleading*, where leading is the description of the jet within the combination of two jets with the higher value of that coordinate and subleading for the lower value. For example, $p_{T,\text{lead}}$ is the transverse momentum of the jet with the higher transverse momentum and $p_{T,\text{sub}}$ is the transverse momentum of the jet with the lower transverse momentum. This distinction can be made for all the jet coordinates p_T, η, ϕ and m.

The momentum fraction within jets, Equation 7, can be extended to the momentum fraction between jets. That is the momentum fraction

$$z = \frac{\min\left(p_{T,i}, p_{T,j}\right)}{p_{T,i} + p_{T,j}}, \tag{8}$$

where i and j are now two jets instead of particles within a jet. The momentum fraction z allows direct measurements of fundamental building blocks of QCD [25]. With the momentum fraction, the generalised angularities in Equation 6 can be extended to jet-level, to define variables that contain information about the hard scattering particles. These aggregated

Table 1: Summary of the discussed characteristics of hard scattering particles. Characteristics are grouped by origin and where they hold information about. There is no necessary link within the rows.

Leading jet	Subleading jet	Combined jets	Aggregated
m_{lead}	m_{sub}	m_{inv}	$z\Delta R$
$p_{T,\text{lead}}$	$p_{T,\text{sub}}$	$p_{T,\text{comb}}$	$z\Delta R^2$
η_{lead}	η_{sub}	ΔR	
ϕ_{lead}	ϕ_{sub}	z	

characteristics are $z\Delta R$ and $z\Delta R^2$, where ΔR is the angle between two jets. Two jets originating from the same particle with a high $p_{T,comb}$ will have a small ΔR because the conservation of momentum keep the jets in the same direction. For small $p_{T,comb}$, two jets will have a high ΔR.

To summarise, we have fourteen characteristics to describe the combination of two jets and therefore the hard scattering particles. Eight of them are the jet coordinates p_T, η, ϕ and m of both the leading and subleading jet. Combining the jets gives us four characteristics. Those are the combined transverse momentum of the jets $p_{T,\text{comb}}$, the invariant mass of the hard scattered particle m_{inv}, the angle between the combined jets ΔR the momentum fraction of the combined jets z. These characteristics can be combined for two aggregated characteristics, $z\Delta R$ and $z\Delta R^2$ which are based on the generalised angularities. A schematic overview of all the discussed characteristics is shown in Table 1.

W bosons are characterised by their mass of 80.376 ± 0.033 GeV [26]. The jet coordinates η and ϕ of the leading and subleading jets will not characterise anything of the W boson. They are just the direction in which the jets are going. But the angle ΔR between them can give us interesting results. It may be that the jets originating from W bosons stay closer to each other than dijet events. The mass distribution between two jets, so the relative ratio between m_{lead} and m_{sub} may also be different for W bosons than for dijet events. This could be likewise for the p_T distribution of two jets. This effect will be visible in the ratio between $p_{T,\text{lead}}$ and $p_{T,\text{sub}}$, but also in z. Underlying structures can become visible when combining the transverse momentum in $z\Delta R$ and $z\Delta R^2$.

3 Experimental setup

To study the collisions at ALICE, the event generator PYTHIA [27] is used. It simulates the collisions at high energies between elementary particles. PYTHIA contains the theory and models for various physics aspects based on recent theoretical insights and the results are fine-tuned with experimental results. PYTHIA can 'force' to produce specific particles in an event. By doing this, one specific process in an event can be studied which can be hard do study in experimental data. While PYTHIA is based on the latest knowledge of QCD, it does not take jet quenching into account. JEWEL [28] is a event generator like PYTHIA. It simulates QCD jet evolution in heavy-ion collisions. JEWEL relies heavily on PYTHIA but it does take jet quenching into account.

The results of the event generator are like the experimental results but on parton level. Momentum and energy of the final particles is known, but the particles are not assigned to jets yet. The software package FastJet [23, 29] provides a broad range of jet finding and analysis tools. FastJet offers both types of jet algorithms as mentioned in Section 2.6. The anti-k_t jet algorithm, which is a sequential recombination algorithm, is used. The distance measures are given by

$$d_{ij} = \min\left(1/p_{Ti}^2, 1/p_{Tj}^2\right) \Delta R_{ij}^2/R^2, \tag{9}$$

$$d_{iB} = 1/p_{Ti}^2, \tag{10}$$

with p_T and ΔR respectively the transverse momentum and angle between two particles, as in Equation 1 and 5 [23]. A jet radius R of 0.4 is used.

ROOT [30] is a data analysis framework developed at CERN and is used for data processing, statistical analysis, visualisation and storage. It is widely used by high energy physicists. ROOT offers a lot of possibilities and can take the input of the previous named software. The data of the events generated by PYTHIA or JEWEL and adapted by FastJet, can be analysed with ROOT.

4 Analysis

4.1 Event generation

PYTHIA is used to generate events of proton-proton collisions with a centre of mass energy $\sqrt{s_{NN}} = 5.02$ TeV. To have a initial feeling of how W bosons behave, we force PYTHIA to create two W bosons as the hard scattering with various $\hat{p_T}$. $\hat{p_T}$ is the minimum invariant p_T of the two hard scattering particles. FastJet reconstructs the jets after the events are generated. To obtain the characteristics of the hard scattering particles, as summarised in Table 1, all combinations between jets within an event are being made. While doing this, all the characteristics are calculated in ROOT.

PYTHIA creates a double W boson pair when two quarks collide, but these are not the only particles created. In a pp collision there are more particles collided than only one quark-quark collision. These collisions are *underlying events*. These will create background in the signal of the results. Besides that, when making combinations between the jets, combinations of jets originating from different hard scattering particles are made. The background in the results of these events is *combinatorial background*. To immediately cut away a part of the background, only combinations of jets are taken in consideration that have a $p_{T,comb}$ that is 10 GeV higher than $\hat{p_T}$. This cut, together with an η cut, will be referred as the *initial cut*:

$$p_{T,comb} > \hat{p_T} + 10, \quad |\eta| < 2.5. \tag{11}$$

The initial cut will be applied on all future events. Although the ALICE detector has a acceptance of $|\eta| < 0.9$, as discussed in Section 2.2, a wider acceptance similar to the acceptance of ATLAS and CMS is used. Detections on the QGP would be performed at ALICE, but detections on W bosons are probably performed at ATLAS of CMS. Therefore is chosen of the $|\eta| < 2.5$.

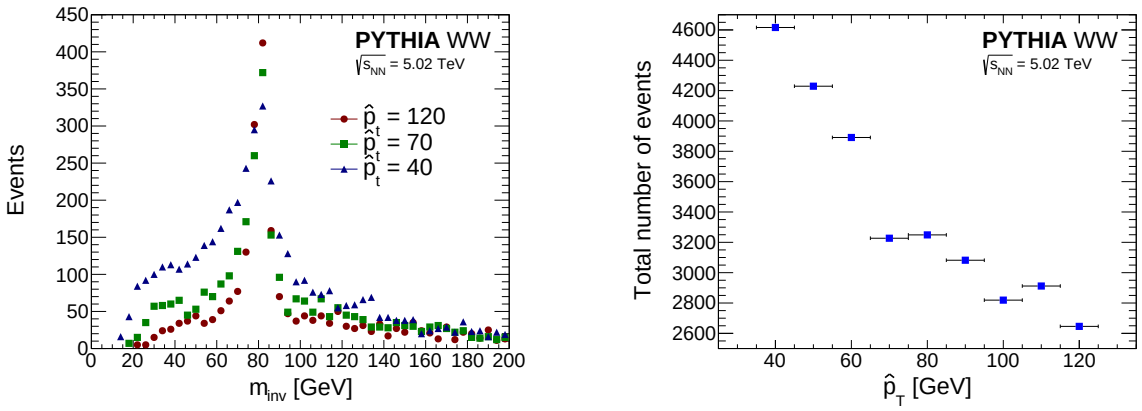

(a) Invariant mass distribution with $\hat{p_T} = 120$, 70 and 40

(b) Total number of events for varying $\hat{p_T}$

Figure 5: Invariant mass distribution and total number of events for PYTHIA generating WW events. The W boson mass peak is more distinct for higher $\hat{p}_T$ but meanwhile the total number of events decreases. Too high $\hat{p}_T$ can mean too few statistics. A compromise between the two has to be made. The mass distributions for all the various $\hat{p}_T$'s are shown in Figure A.1.

The invariant mass distribution is shown for three different $\hat{p_T}$ in Figure 5a, the invariant mass distributions of all different $\hat{p_T}$ are shown in Figure A.1. In Figure 5b, the total number of events per $\hat{p_T}$ of the invariant mass distributions is shown. The total number of events is decreasing for higher $\hat{p_T}$ because of the cut of $p_{T,comb} > \hat{p_T} + 10$. This does not give any problems for the higher $\hat{p_T}$'s in Figure 5, but this will be the case if there are more cuts on the events, which will come later. The background is increasing for lower $\hat{p_T}$ and the peak around the W boson mass gets less distinct. To find an equilibrium between enough events and a distinct peak, $\hat{p_T} = 70$ is chosen.

4.2 Fit

The peak around 80 GeV in the mass distribution is a Gaussian while the background does not have a specific shape. We will describe the mass distribution as a Gaussian plus a polynomial. This Gauss + polynomial fit function is shown in Figure 8a with a fourth order polynomial. A fit with other order polynomials are shown in Figure A.2. The polynomials are ranging from second order to seventh order. The fitting is being helped by setting the region of the mean and the width of the Gauss to (72, 86) and (0, 10) respectively. The fit procedure of each graph is being repeated for hundred times while the fit parameters start to search at the values of the fit parameters of the previous fit iteration. In Figure A.2 we see that almost all the different fit functions do a good job. To determine which is the best, a Monte Carlo method of pull distributions is used.

Pull statistics are used in the method of extended maximum likelihood fit and it can be superior to a regular maximum likelihood fit [31]. A (simplified) way of defining the pull

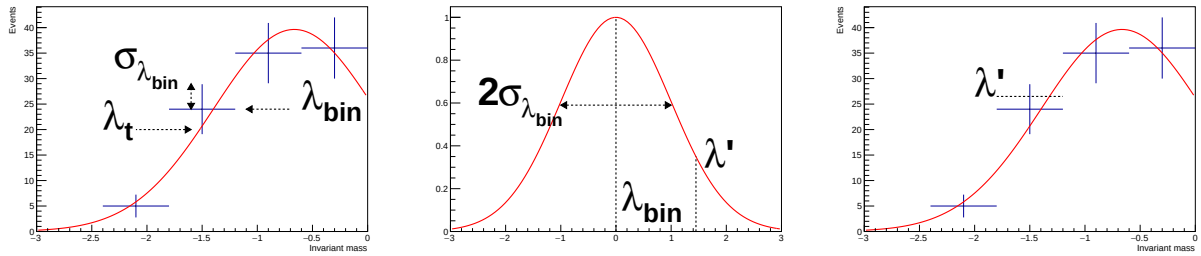

(a) The fit and its data points **(b)** The random value λ' from a data point **(c)** The random value in the fit

Figure 6: Sketch of the main steps in determining the pull distribution with pseudo-experiments of a fit. A fit has the value λ_t at a location where the data point has the value $\lambda_{\text{bin}} + \sigma_{\lambda_{\text{bin}}}$. A random value λ' is determined from a Gaussian around λ_{bin} with $\sigma_{\lambda_{\text{bin}}}$ as the width. This random value λ' is subsequently compared with the fit value λ_t.

statistic is as

$$p = \frac{\lambda' - \lambda_t}{\sigma_{\lambda'}}, \tag{12}$$

where λ_t is the true value and $\lambda' \pm \sigma_{\lambda'}$ is the result of one particular pseudo experiment. To get a pull distribution of the fits in Figure A.2, the pull statistic from Equation 12 is calculated multiple times. The true value λ_t is the value of the fit at the location of the bin, as shown in Figure 6a. The result of a simplified pseudo experiment λ' is calculated by generating a random value according to a Gaussian with mean λ_{bin} and width $\sigma_{\lambda_{\text{bin}}}$ [32], where $\lambda_{\text{bin}} \pm \sigma_{\lambda_{\text{bin}}}$ is the value and its error of a bin in the mass distribution, as is done in Figure 6b. The result of this random value can be placed in the original graph, as in Figure 6c. Equation 12 repeated $N = 10^4$ times for every bin. This will distribute the pull statistics as a Gaussian. The mean and the width, which are shown in Figure 7, of the Gaussian describe the quality of the fit function. For a mean closer to zero and a smaller width, the fit function has a better quality. The fits of the mass distribution with different polynomial orders are shown in Figure A.2. The pull distributions of these fits are shown in Figure A.3. From Figure 7 it becomes clear that a fourth order polynomial describes the background the best. So a Gaussian plus a fourth order polynomial will describe the mass distributions.

4.3 Constituent subtraction

When forcing PYTHIA to create W bosons, of course the mass peaks around 80 GeV will be clearly visible. W bosons are also created when they are not forced to create in PYTHIA, but way less frequently. Before trying to find them in those events, we will try to find specific regions of the characteristics where W bosons are created. We do this by adding underlying events, which are thermal events from the CERNBox [33] with independent particles using a Boltzmann distribution with a fixed multiplicity of 4500 and mean $p_T = 1$. Multiplicity is a measure of the number of hadrons produced [34]. Higher multiplicity means more particles in a event which results in more background.

These thermal events are added to the signal events and subsequently subtracted. The

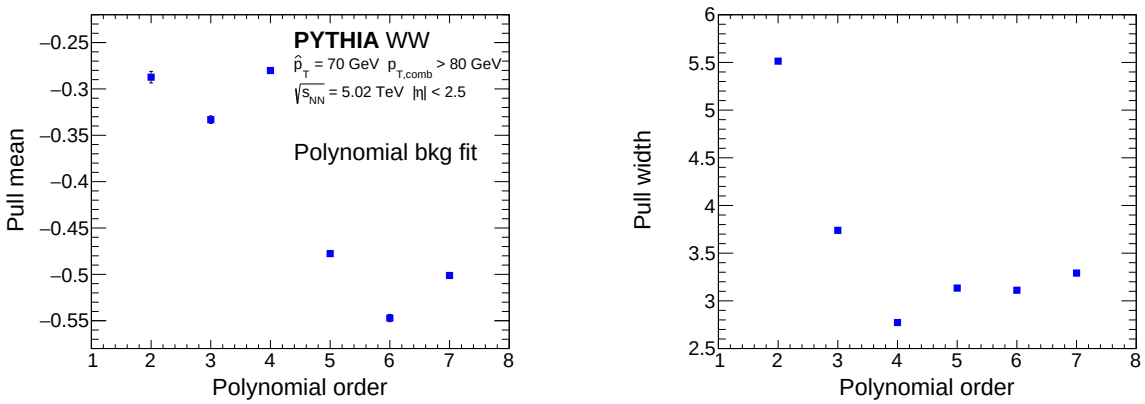

(a) The mean of Gaussian that fits the pull distributions.

(b) The width of Gaussian that fits the pull distributions.

Figure 7: The statistics of the Gaussian that fits the the pull distributions of the WW mass distribution with varying fit functions of the form Gaussian + polynomial. For polynomial orders from two trough seven are fit functions applied. The pull distributions themselves are fitted by a Gaussian. The mean and width of these Gaussian's is shown. Both graphs do have error bars but these are often too small to see. The fits are shown in Figure A.3.

reason for this is that the subtraction of the events is done by an algorithm that does not do a perfect job. In this way the signal is diluted with more background in a way it would also be in reality. The subtraction method is the constituent subtraction method. Following the discussion of [35], massless ghosts particles are added to the event so that each jet will contain real and ghost particles. For every combination of real and ghost particles, the distince similar to Equation 5 is calculated. Starting at the particle-ghost pair with the smallest distance, the transverse momentum of both particles is calculated. If the transverse momentum of the particle is higher than that of the ghost, the transverse momentum of the ghost is subtracted from the real particle and the ghost is discarded. If the transverse momentum of the ghost is larger than the particle, the transverse momentum of the ghost is corrected and the real particle is discarded. The mixed events that end up after the subtraction are called *constituent subtracted* events because of its method. The unmixed events, that we were already using are called *signal* events.

Figure 8 shows the mass distributions of the original the signal and constituent subtracted events. In comparison with the signal events, the constituent subtracted events have more events with a lower invariant mass. The main difference is that the W boson peak is much wider and lower, as can be expected. The jets originating from W bosons have particles of the underlying events in them, making their invariant mass different. The constituent subtracted mass distribution is a stepping stone to the comparison with dijet events. By studying the constituent subtracted events we can do predictions about the behaviour of W bosons in dijet event data.

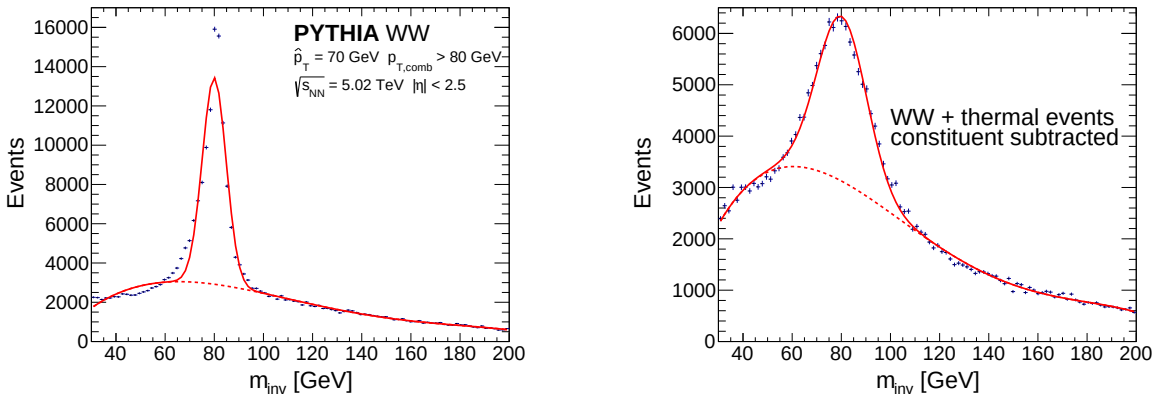

(a) Signal events

(b) Events with additional thermal events that are constituent subtracted

Figure 8: Mass distributions of signal events and constituent subtracted events where thermal events with a multiplicity of 4500 and mean $p_T = 1$. The constituent subtracted thermal events mimic the background of WW events and spread the W mass peak out.

4.4 Response ratio

The response ratio is calculated by dividing a characteristic of the constituent subtracted events by the signal events. Because we want to distinguish W bosons in the invariant mass distribution, the response ratio of the invariant mass is calculated. Since the constituent subtracted jets and the signal jets are originating from the same events, no further matching is needed. This is confirmed by Figure 9, where the ΔR between the constituent subtracted and signal jets is shown. The distance between the jets is always small enough to assume that the jets are still the same jet.

The response ratios are the values of the divisions of the invariant masses of the constituent subtracted and signal jets. The histogram of the response ratios will form a Gaussian with its mean around one. The mean of the Gaussian is called the *scale* and the width the *resolution*. The shape of the Gaussian describes the similarities of the constituent subtracted and signal events. When the scale is closer to one and the resolution is smaller, the events are in more correspondence with each other. The scale and resolution are calculated varying the characteristics summarised in Table 1. The aim of this is to cut away the regions of the characteristics where the scale is not close to one and/or the resolution is high. The regions of the characteristics where the responses are calculated are determined by the number of events in the bins within the region. There can not be too few events in a bin region, otherwise there are not enough events to form the Gaussian's of the response ratios.

All scales are above 0.95 and below 1.00 as shown in Figure A.5. Due to the fact that all scales are close enough to one we can consider that the signal and subtracted events are similar enough to compare the two between each other. The resolution tells us more about the comparison between them. The lower it is, the less the signal and constituent subtracted events are differing. In Figure 10 we see that the resolution drops for higher masses. This is what could be expected. The lower energy particles from the soft scattering

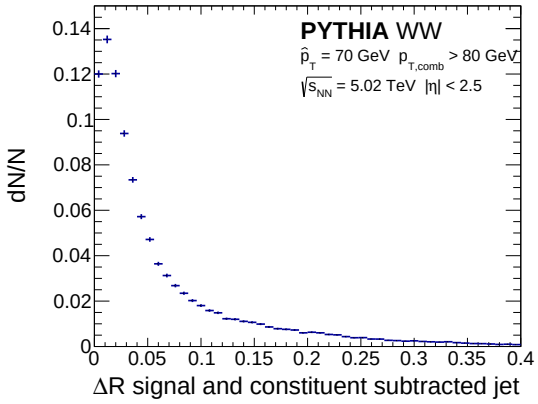

Figure 9: The angle ΔR between the signal and constituent subtracted jets. For almost all the jets $\Delta R < 0.4$. It is safe to assume that the jets are still the same jets and no further matching is needed.

of thermal events can not produce particles with high masses, while the particles from the hard scattering in the signal events can produce higher mass particles. Especially the subleading mass stands out because the resolutions divides itself by almost four over the span of around $m_{\text{sub}} = 10$ GeV. This indicates that the subleading mass could be a good characterisation to distinguish W bosons. The sudden trench in the resolution around $m_{\text{inv}} = 80$ GeV could also be expected. In fact, it would be worrying if it was not there. In Figure 8 there is a sharp peak around $m_{\text{inv}} = 80$ GeV for the signal events as well as for the constituent subtracted events, although it is more spread out for the latter. The drop of resolution around that invariant mass indicates the signal and constituent subtracted events have more similarities around $m_{\text{inv}} = 80$ GeV than higher and lower invariant masses.

In Figure 10 are also the resolutions of the transverse momenta shown. The behaviour of the resolution of the leading transverse momentum is odd. It peaks around $p_{T,\text{lead}} \approx 100$ GeV and decreases for higher and lower momenta at more or less the same rate. The scale follows a similar but opposite pattern. So the peak of $p_{T,\text{lead}}$ is probably because of the quality of the response ratio and not due to physical aspects. A further investigation of the leading transverse momentum without using the response ratio will be discussed later. The subleading transverse momentum follows a similar pattern as the subleading mass. The resolution drops like an exponential decay for higher momenta. This indicates that $p_{T,\text{sub}}$ could be a good characterisation to distinguish W bosons. The resolution decreases too for higher combined transverse momentum. The reason of this is similar to the decrease of resolution for higher masses. The soft scattering of the thermal events do not produce particles with high transverse momentum, while the W bosons do.

The difference between the highest and lowest value of the resolution when varying the mass and transverse momentum is very roughly the same for the leading jet. It peaks for both the leading mass (Figure 10a) and leading transverse momentum (Figure 10e) around 0.25 and is the lowest around 0.15. The same is very roughly true for the subleading mass (Figure 10b) and the subleading transverse momentum (Figure 10f) with 0.3 at its maximum and 0.05 at its minimum. It holds as well for the combination of jets, the invariant mass

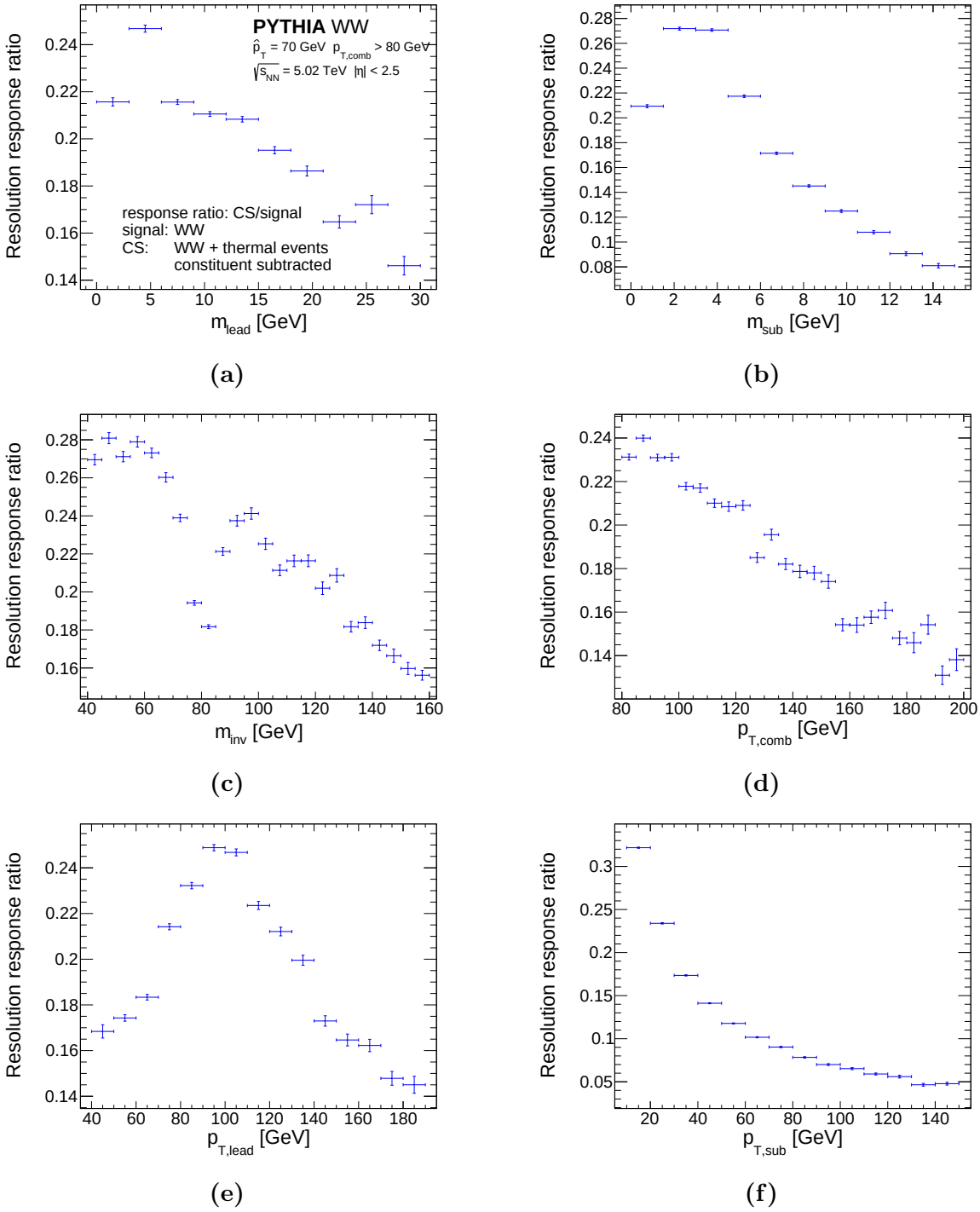

Figure 10: Resolution of the signal and constituent subtracted events of the masses and transverse momenta. Generally speaking, the resolution gets lower and therefore better for higher values. A drop in resolution is observed around $m_{\text{inv}} = 80$ GeV. That is expected because both the signal and subtracted events have a peak around that invariant mass, as shown in Figure 8.

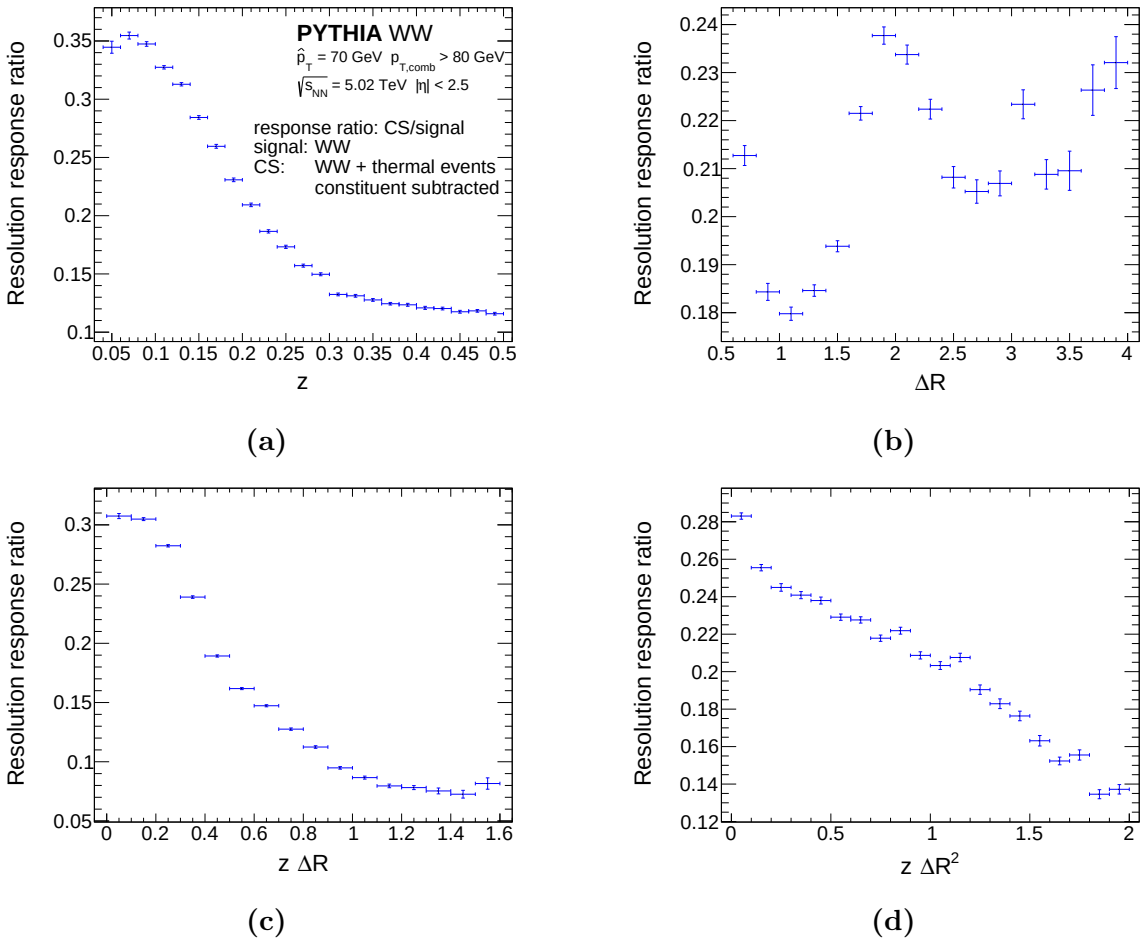

Figure 11: The resolution of the angle ΔR, momentum fraction z and aggregated characteristics $z\Delta R$ and $z\Delta R^2$. Besides the ΔR, all resolutions seems to give good results. They decrease when the characteristic is increased, indicating that W bosons are better distinguishable at higher values of these characteristics. The resolution of ΔR does not have a clear behaviour and needs further investigation.

(Figure 10c) and combined transverse momentum (Figure 10d) with 0.25 and 0.15. If the relative difference between two values is defined as

$$d(x, y) = \left| \frac{x - y}{(x + y)/2} \right|, \tag{13}$$

the relative difference between the highest and lowest value of the resolution of the leading, subleading and combined jets is very roughly 0.50, 1.4 and 0.50, respectively. The relative difference of η and ϕ are much lower in this way, around 0.12, as shown in Figure A.4. The resolution does not have a strong dependence on the leading or subleading jet, of both η and ϕ. This is expected, because the direction of scattering should not depend on the particles (W bosons or thermal events). This means that η and ϕ are not good characterisations of W bosons.

Although W bosons are not distinguishable by the direction of the single jets they produce,

the difference between the direction could potentially be a good characterisation. The angle between the decaying particles that form jets could be different, depending if they decay from a W boson, thermal events or some other particle. This is not what Figure 11b is showing us. The response resolutions does not give us any useful insights about ΔR. To investigate further how ΔR is behaving after mixing with and constituent subtraction of thermal events, the distribution of ΔR is, in combination with the invariant mass, shown in Figure 12. This is done for $p_{T,\text{lead}}$ as well, where the response ratio also did not give insightful results. The difference between the signal and constituent subtracted events is similar between ΔR and $p_{T,\text{lead}}$. For the signal events we see a peak around the W boson mass that spreads out over a large region of ΔR and $p_{T,\text{lead}}$. The constituent subtraction spreads the peak of invariant mass out, just the same as we see in Figure 8. The region of ΔR and $p_{T,\text{lead}}$ get squashed together and the W bosons center approximately between $1 < \Delta R < 2$ and $60 < p_{T,\text{lead}} < 120$, although the latter is of course also depended on $\hat{p}_T$.

The resolutions of z and the aggregated combinations $z\Delta R$ and $z\Delta R^2$ in Figure 11 show good results. This is not surprising since z and $p_{T,\text{sub}}$ are closely related. When comparing the three, it becomes clear why aggregated combinations can be useful. The resolution of $z\Delta R$ has a steeper decline and becomes even closer to zero that z only. The aggregated combination $z\Delta R^2$ also shows a clear result that for higher values the resolution decreases, but not as good as $z\Delta R$.

The discussion of the resolution of the response ratio learnt us that the different jet characteristics behave different when they are varied. The best en clearest characteristics to distinguish W bosons are the subleading mass m_{sub}, the subleading transverse momentum $p_{T,\text{sub}}$, the momentum fraction z and the aggregated combination $z\Delta R$. They showed to distinguish W bosons better at higher values. These jet characterisations will be compared to dijet background samples.

4.5 Dijet events

To compare WW signal events with the background, dijet events are created in PYTHIA. The same $\hat{p}_T$ and initial cut (see Equation 11) are applied to these events. Besides WW events, Wq and Wg events also create W bosons, so they are also created and added to the WW events to create the full signal. All events have their own cross section in a hard scattering. So the events should be scaled with their own cross-section before adding and comparing them. PYTHIA gives the following cross-sections for the events:

$$\begin{aligned} \sigma_{WW} &= 3.2 \times 10^{-9}\,\text{mb}, \\ \sigma_{Wq,Wg} &= 5.2 \times 10^{-7}\,\text{mb}, \\ \sigma_{dj} &= 9.0 \times 10^{-4}\,\text{mb}. \end{aligned} \tag{14}$$

Where the subscript dj stands for dijet and mb is a millibarn which is equivalent to $10^{-31}\,\text{m}^2$. The mass distributions are shown in Figure 13. The full picture is obtained by stacking the three graphs. Because the cross section of the dijet events is so much larger than the other two, it is not possible to distinguish the W bosons in the stacked graph. Dijet events are way more often measured because of the larger cross section. To distinguish the W bosons in the stacked graph, cuts based on the response ratio will be applied.

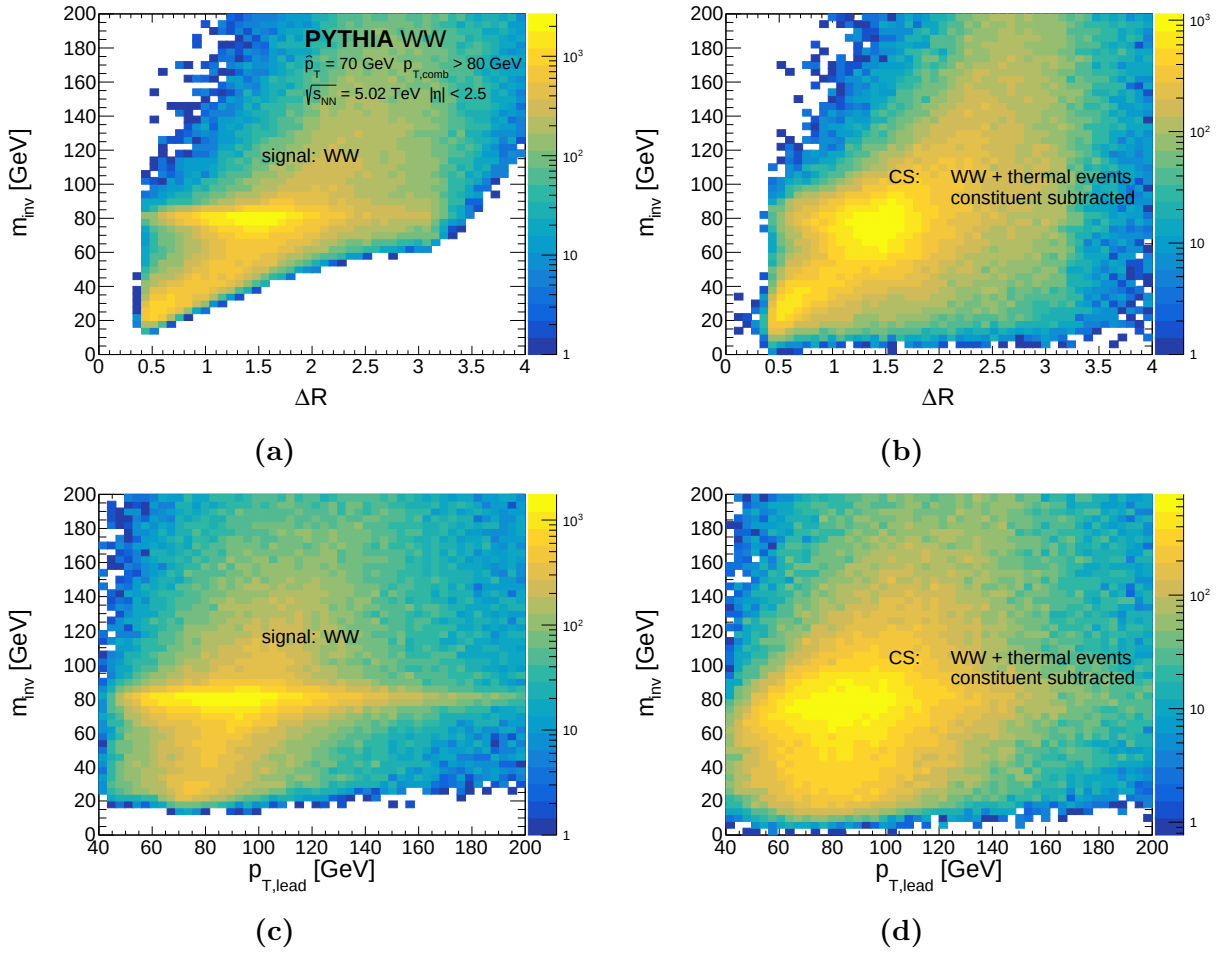

Figure 12: Two dimensional histograms of m_{inv} versus ΔR (Top) and $p_{T,\text{lead}}$ (Bottom) with WW signal events (Left) and with thermal events constituent subtracted (Right). The mixing with and constituent subtraction of thermal events has the same influence on ΔR and $p_{T,\text{lead}}$. After the constituent subtraction the peak is only distinct in one region, while before in the signal events the peak around the W boson mass was present over almost the entire range.

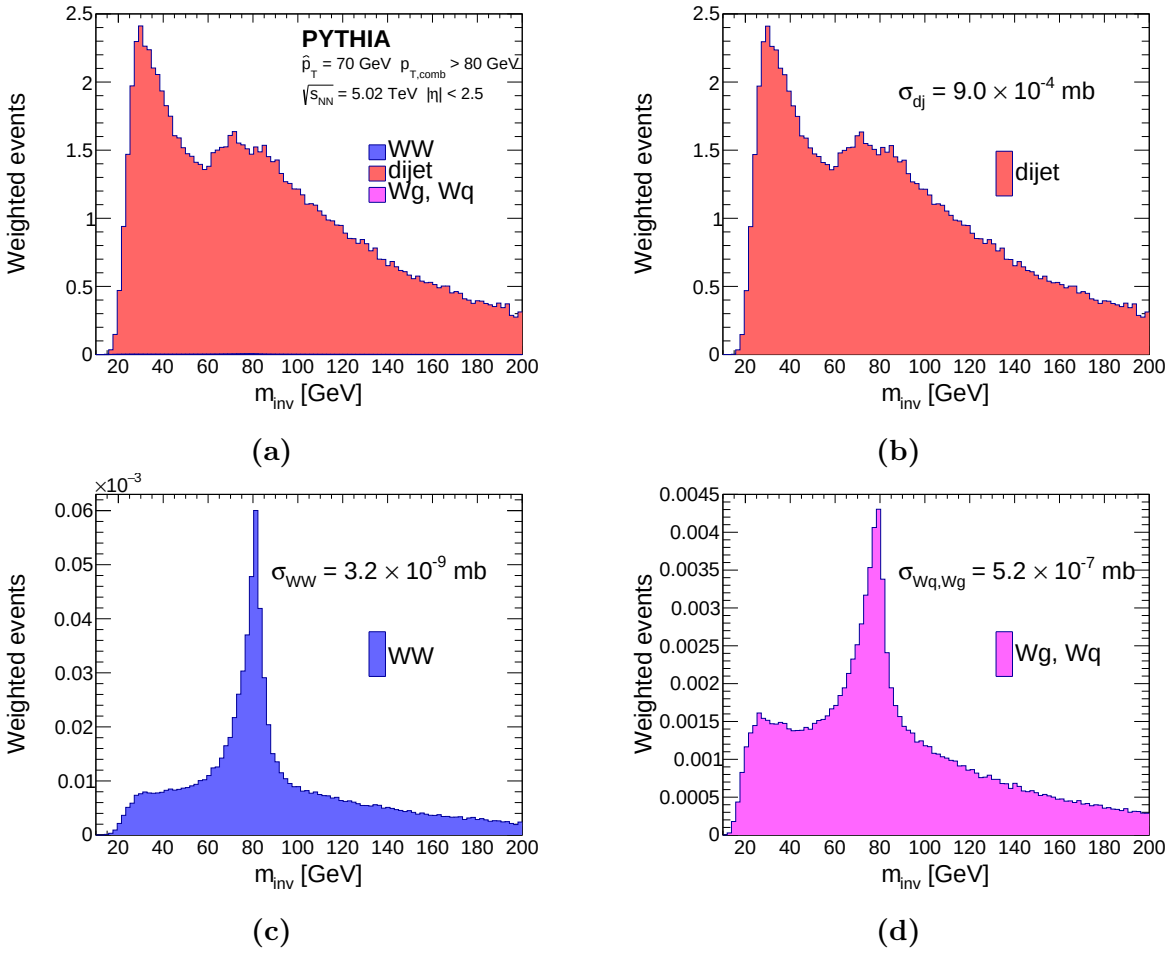

Figure 13: Mass distribution of the WW, Wq Wg and dijet events stacked (Top left) and split. The signal events (WW, Wg, Wq) are present in the stacked graph, but are not visible because of the higher cross section of the dijet events. The events are weighted by their cross section. The signal events are quite similar with a high peak around the W boson mas. The dijet events also have a peak around 80 GeV but this is due to $\hat{p}_T = 70$ and the cut of $p_{T,\text{comb}} > 80$ and should not be considered as part of the W boson signal.

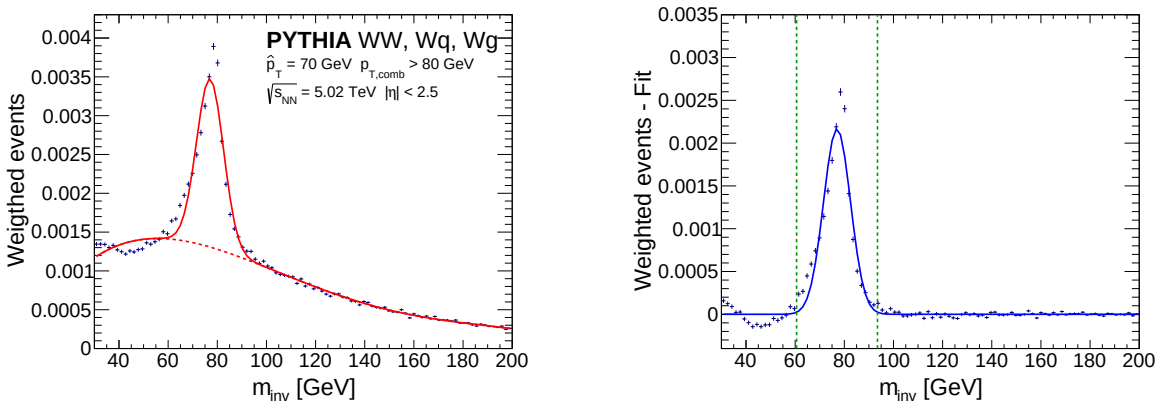

(a) Signal events **(b)** Signal events minus background fit

Figure 14: The mass distributions of the signal events WW, Wq and Wg, scaled by their cross section. The region between the green lines is the Gaussian region $\mu \pm 3\sigma$.

To determine how good the W bosons in the signal (WW + Wq + Wg events) are distinguishable from the background (dijet events), the statistical significance of the observed signal $S/(\sqrt{S+B})$ and the signal-over-background ratio S/B are used. We want to optimise the significance with the condition that the S/B ratio does not get to low. The determination of the signal S and background B is as follows. As usual, a Gaussian + polynomial is fitted to the signal events, as in Figure 14a. The value of the polynomial background is subtracted from the bin contents so only the Gaussian remains, as in Figure 14b. The signal S is the sum of the bin contents within the range of $\mu \pm 3\sigma$, where μ and σ are the mean and width of the Gaussian, respectively. So the bin contents between the green lines are summed. The background B consists of the same m_{inv} region as used for the signal S, but the bin contents of the dijet events are now summed. When a cut is applied, this fit procedure is repeated to determine the new invariant mass region where the S and B should be determined from.

In the discussion of the response ratio was concluded that with higher minimal cuts of m_{sub}, $p_{T,\text{sub}}$, z and $z\Delta R$, W bosons were easier to distinguish. The S/B ratio and significance are shown in Figure 15, where the lower regions of the just named characterisations are cut away. To really conclude anything useful, both the S/B ratio and significance have to be higher than three. This is by far not obtained because of the big difference between the cross section. But the behaviour of the S/B ratio and significance when varying the cuts will be useful. Because of the decrease in resolution for higher cuts, the S/B ratio is expected to increase for higher cuts. This is not what is happening for the subleading mass, as is shown in Figure 15a. This means that the signal is cut away faster than the background when increasing the minimal value of the subleading mass. Even the significance in Figure 15b starts immediately to decrease when applying cuts. This means that there should be no minimal cuts applied to the subleading mass. The ratio of the subleading transverse momentum gives us more promising results in Figure 15c. The ratio starts and keeps increasing when higher cuts of $p_{T,\text{sub}}$ are applied. So jets originating from W bosons have generally speaking a higher $p_{T,\text{sub}}$ than jets originating from quarks. But Figure 15d tells us that we can not keep increasing $p_{T,\text{sub}}$ for the sake of distinguishing W bosons. The

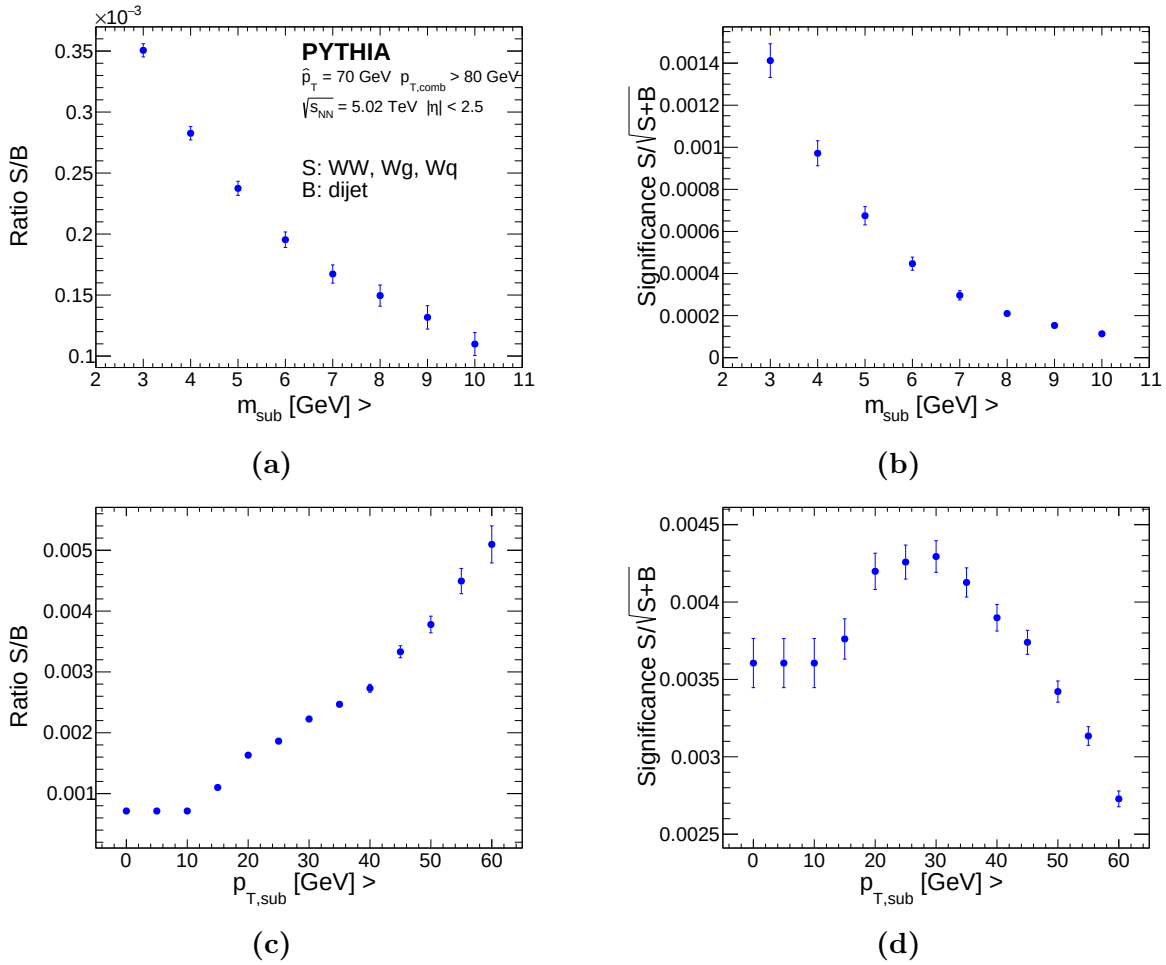

Figure 15: S/B ratio and significance of the invariant mass with minimal cuts on m_{sub} and $p_{T,\text{sub}}$. The x axis means the minimal value that jets should have to be taken into account. The S/B ratio and significance of m_{sub} both decrease for higher minimal cuts, so no minimal cuts should be applied. The S/B ratio of $p_{T,\text{sub}}$ increases for higher minimal cuts, but the significance starts to decrease after a peak for higher minimal cuts.

significance of $p_{T,\text{sub}}$ starts increasing when applying the first cuts and peaks at $p_{T,\text{sub}} > 30$. This means that this minimal value of $p_{T,\text{sub}}$ is the best when looking for W boson at $\hat{p}_T = 70$. The behaviour of the S/B ratio and significance of z and $z\Delta R$ is similar to $p_{T,\text{sub}}$ and therefore not further discussed. They are shown in Figure A.6. The similarities could be expected since $p_{T,\text{sub}}$ and z are closely related. The height and width of the significance peak has different values but the shape is similar.

Applying minimal cuts to characteristics depending on transverse momenta like we did makes sense. More W bosons are created at higher transverse momenta while the thermal are not. Jets stay closer to each other if they have higher transverse momenta to maintain the transverse momenta of their parent particle. If jets stay closer to each other, they have a smaller angle ΔR between them. Because W bosons are more distinguishable at higher p_T, they should also bee more distinguishable at lower ΔR. Although the response ratio did not show this clearly, we can still study the S/B ratio and significance for ΔR. These are

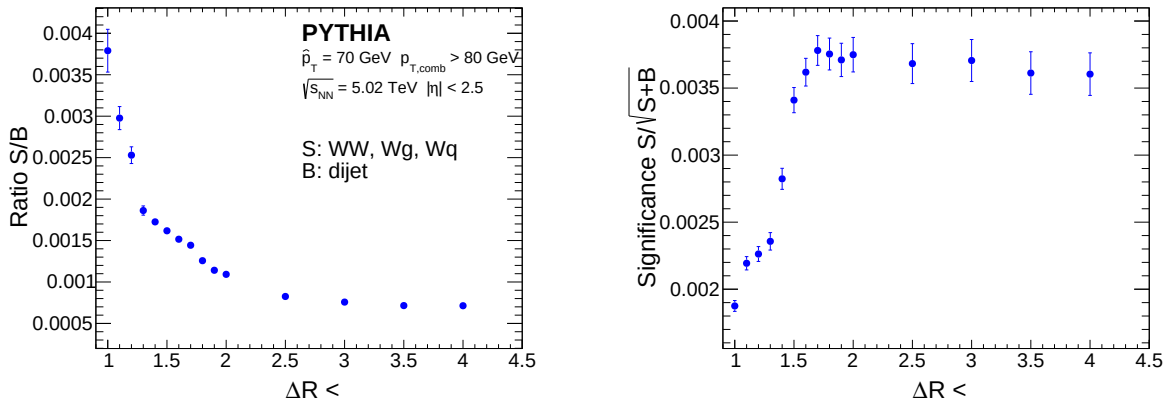

(a) **(b)**

Figure 16: S/B ratio and significance of the invariant mass with maximal cuts on ΔR. The x axis is the maximal value of jets that have to be taken into account. Lower maximal cuts give a higher S/B ratio but lower significance. The significance stays more or less stable after maximal cuts of $\Delta R < 1.7$.

shown in Figure 16 for maximal cuts, so all jets with a value smaller than a certain ΔR. What we see is that the exchange between S/B ratio and significance we saw for transverse momenta is flipped. Smaller ΔR results in a higher S/B ratio but simultaneously also in a lower significance. The maximal cuts are only applied up to $\Delta R < 1$ and not lower, because otherwise there are too few events in the signal and background events. The S/B ratio starts immediately to decrease like an exponential decay. The significance doubles approximately between $\Delta R < 1$ and $\Delta R < 1.7$ and after that stay more or less constant.

So far, several regions of characteristics are established when distinguishing W bosons from dijet events. The S/B ratio and significance of the subleading mass showed that there should no minimal cuts be applied to it. The S/B ratio of $p_{T,\text{sub}}$, z and $z\Delta R$ is always increasing for higher minimal cuts but the significance peaks in small regions of these characteristics. The S/B ratio of ΔR is the highest for lower angles while the significance growths rapidly when increasing minimal cuts but stays constant after $\Delta R \approx 1.7$. This is summarised in Table 2, including the specification where the significance is at its peak. These cuts will be combined in a multi-variable analysis to obtain the final results. By combining cuts in a wrong way, the S/B ratio and significance can decrease. This can happen when jets with a cut in characteristic one have a high S/B ratio and significance, while those jets have a low S/B ratio and significance when they are also cut in characteristic two. Even when only cutting with characteristic two will increase the S/B ratio and significance. To prevent this, the S/B ratio and significance when combining characteristics are discussed in the next section.

4.6 Multi-variable analysis

We have analysed the difference between the jet characteristics of W bosons of signal and constituent subtracted events with the response ratio. Based on those differences, the S/B

Table 2: Summary of the established cuts where S/B ratio and significance are are at its best. $>$ ($<$) after a jet characteristic indicates that minimal (maximal) cuts are applied. $>>$ ($<<$) indicates that higher (lower) cuts give the best S/B ratio. The value of the characteristic of the most right column gives the value where the significance is the highest.

Jet characteristic	S/B ratio	Significance
$m_{\text{sub}} >$	$<<$	0 GeV
$p_{T,\text{sub}} >$	$>>$	30 GeV
$z >$	$>>$	.2
$z\Delta R >$	$>>$	0.25
$\Delta R <$	$<<$	1.7

ratio and significance as quantification of the distinctness of W bosons in dijet events are studied by varying the jet characteristics. These cuts in the jet characteristics have been summarised in Table 2. Combining these cuts in a right way increase the S/B ratio and significance and consequently will improve the distinctness of W bosons.

The behaviour of the S/B ratio and significance when combing multiple characteristics can not be easily shown in a graph, because the number of characteristics exceeds the two or three dimensions than can be visualised in an understandable way. Nevertheless is a visualisation of all cuts shown in Figure 17. It shows that applying *more* cuts results in a higher S/B ratio until a certain level. After that, applying *higher* cuts will only increase the S/B ratio. But applying higher cuts will decrease the significance, and the significance is not always increased by applying more cuts. So *which* combination of cuts is applied is more important for the significance.

The significance of $p_{T,\text{sub}}$, z and $z\Delta R$ have a similar peak in a specific region as can be seen in Figures 15d, A.6b and A.6d, respectively. The latter two are heavily depending on $p_{T,\text{sub}}$ because the value of z is mainly determined by $p_{T,\text{sub}}$. The jets that are in the peak in the significance of z and $z\Delta R$ are the same jets that are in the peak of the significance in the cuts of $p_{T,\text{sub}}$, as can be seen in Figure 18. In fact, the significance of $p_{T,\text{sub}}$ starts to decrease just after the peaks of z and $z\Delta R$. The jets that are taken into account after cuts in z and $z\Delta R$ that result in higher significance are the same jets that have higher significance after the cut in $p_{T,\text{sub}}$. So it is safe to use all three cuts of $p_{T,\text{sub}} > 30$ GeV, $z > 0.2$ and $z\Delta R > 0.25$ at the same time.

Jets with the cuts $p_{T,\text{sub}} > 30$ GeV, $z > 0.2$ and $z\Delta R > 0.25$ all apply a minimal value to some sort of transverse momentum. Jets with higher transverse momenta have a lower angle ΔR. So applying a maximal value with the cut $\Delta R < 1.7$ in combination with the previous cuts in the transverse momenta specify the same kind of jets. In Figure 19b we see that combining those cuts will improve the significance more than when only one cut is applied. We can assume that the same yields when combing cuts $z >$ or $z\Delta R >$ with $\Delta R <$ because the jets in the significance peak of the cuts $z > 0.2$ or $z\Delta R > 0.25$ were the same as in $p_{T,\text{sub}} > 30$. The S/B ratio has not been increased that much in comparison with other cuts of $\Delta R <$, as we see in Figure 19a. But optimising the significance is more important than the S/B ratio so we chose to keep these established cuts.

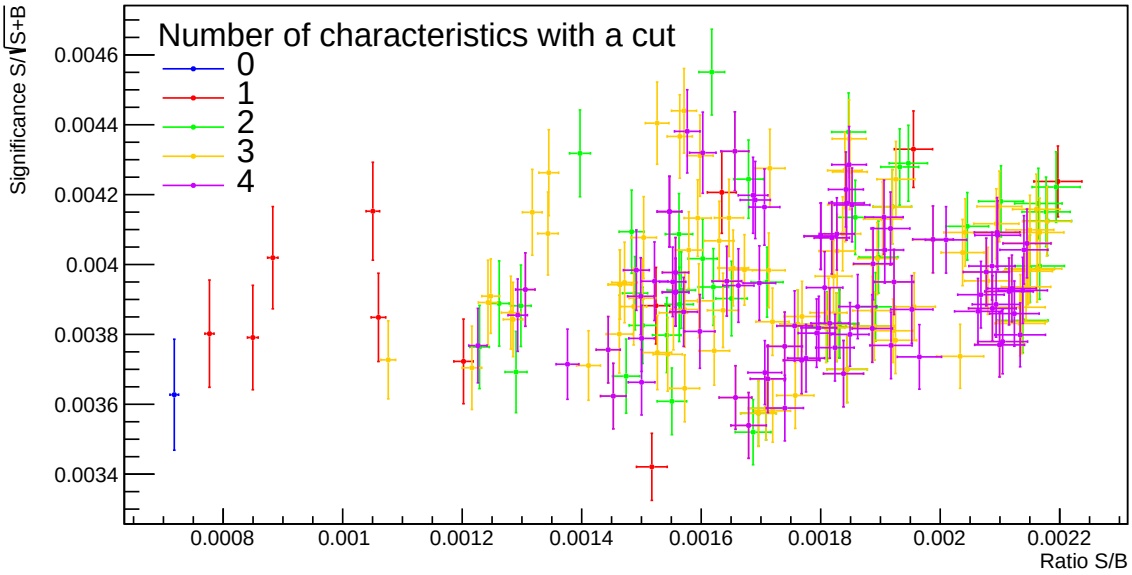

Figure 17: All combinations of the cuts of $p_{T,\text{sub}} > 0, 20, 25, 30$ GeV, $z > 0, 0.15, 0.20, 0.25$, $z\Delta R > 0, 0.2, 0.25, 0.30$ and $\Delta R < 2\pi, 2.5, 2, 1.5$ have been applied on the signal and dijet events. The first cuts (so $p_{T,\text{sub}}$, z, $z\Delta R > 0$ and $\Delta R < 2\pi$) do not count as a cut as there are no jets cut away. The colour depends on the number of characterisations where a cut is applied. The more cuts applied, the higher the S/B ratio. The fully uncut case (the blue one) clearly has the lowest S/B ratio. A few one-time-cut cases (the red ones) follow with relatively the lowest S/B ratio. After that there is a large cluster where no distinct pattern is evident, besides a high density of cases at the highest S/B ratio's. The lack of a clear pattern shows that it is does not matter much *how many* cuts are applied. It is more important *which* cuts are applied. The high density of cases with a high S/B ratio, especially the one with the most number of cuts (the purple ones), indicates that applying more cuts does not have much impact and that the S/B ratio reaches a limit. This limit is because the combination of cuts take the same jets into account, so not much jets are cut limit after a the first few cuts.

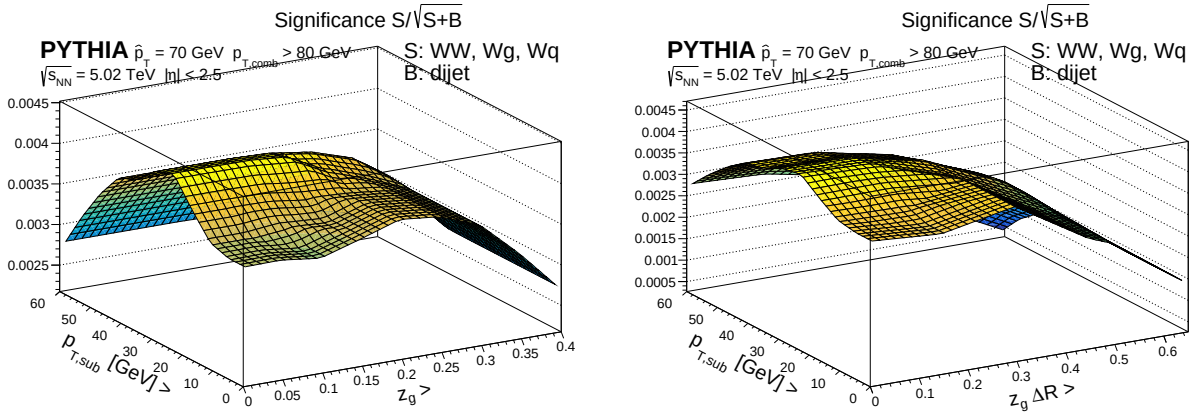

(a) **(b)**

Figure 18: The significance when applying cuts $p_{T,\text{sub}} >$ and $z >$ or $z\Delta R >$. All jets that have a higher value than the specified cut are taken into account, so not a bin or region of this characteristic. The peak of significance when $p_{T,\text{sub}} > 30$ is still present when $z > 0.2$ or $z\Delta R > 0.25$. If one of the cuts is increased, the significance starts to decrease both directions $p_{T,\text{sub}}$ and z or $z\Delta R$.

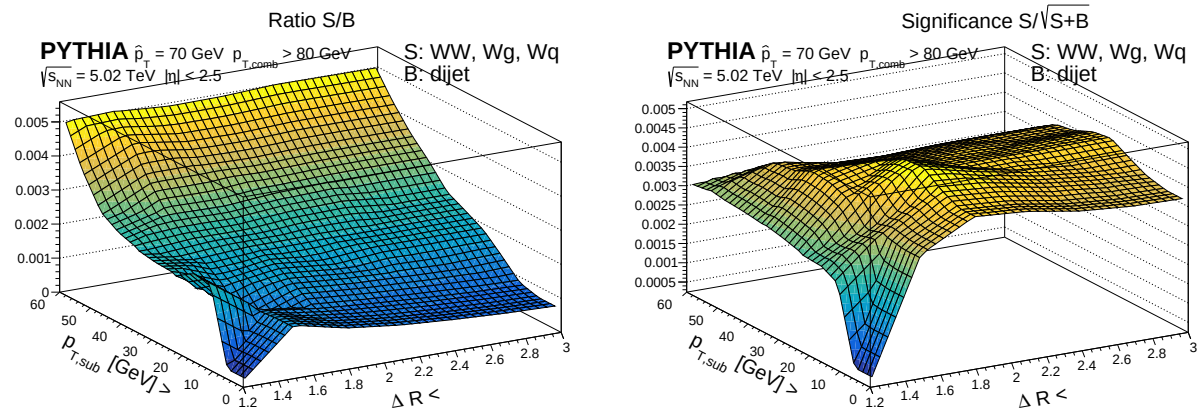

(a) **(b)**

Figure 19: The S/B ratio (Left) and significance (Right) when applying a minimal cut $p_{T,\text{sub}} >$ and maximal cut $\Delta R <$. The S/B ratio increases when for higher $p_{T,\text{sub}}$ and lower ΔR as expected. The significance maximises when two cuts are combined, so they strengthen each other at approximately $p_{T,\text{sub}} > 30$ and $\Delta R < 1.7$.

5 Results

5.1 Dijet events

Applying the established cuts $p_{T,\text{sub}} > 30$ GeV, $z > 0.2$, $z\Delta R > 0.25$ and $\Delta R < 1.7$, as summarised in in Table 2, together with the initial cuts of $p_{T,comb} > \hat{p_T} + 10 = 80$ GeV and $|\eta| < 2.5$, gives a positive result on the S/B ratio and significance $S/\sqrt{S+B}$ when distinguishing W bosons in dijet events. The significance is at its maximum at those cuts. From the multi-variable analysis we found that combining these cuts will even improve the S/B ratio and significance in comparison with applying only one cut. The cuts strengthen each other because they cut their own part of the background away from the the desired W jets.

A comparison between no cuts at all (besides the initial cuts) and the established cuts applied is shown in Figure 20. The S/B ratio and significance of them are shown in the first row of Table 3. The S/B ratio and significance are both in the order of 10^{-3}, without cuts and with the established cuts applied. Although both the S/B ratio and significance are too low to find any W bosons in real measurements, the established cuts have a positive influence on both the S/B ratio and significance. The S/B ratio has more than tripled, from $(0.714 \pm 0.00722) \times 10^{-3}$ to $(3.61 \pm 0.159) \times 10^{-3}$. The significance increases also significantly. Because the physics in particles and jets from collisions is different at higher or lower transverse momenta, the S/B ratio and significance are also shown in Figure 21 for various $p_{T,\text{comb}}$ bins. The S/B ratio increases for higher $p_{T,\text{comb}}$ and with the established cuts applied it increases even more. So for higher $p_{T,\text{comb}}$ the amount of dijet jets decreases in comparison with W boson jets. When the established cuts are applied, the S/B ratio increases more. This proves that the established cuts really focus on W bosons and not on other jets.

5.2 JEWEL

An important process in the QGP is jet quenching, which is not taken into account in PYTHIA, but is in JEWEL. A comparison between the two invariant mass distributions of signal Wq and Wg events is shown Figure 22. Even without the established cuts, the W boson peak is way more distinct in the JEWEL events. There is less background around the peak and the peak is sharper. This is also what we see in the S/B ratio in Table 3. The background B is now the part of the events *under* the Gaussian, so the background fit of the signal, instead of dijet events. The S/B ratio of both PYTHIA and JEWEL has more than quadrupled when the established cuts are applied. So the established cuts cut also a part of the combinatorial background in the signal events away. The significance increases as well, as we see in Table 3. The uncertainty in the S/B ratio is also very high. This is because its inversely depended on background B, which is very small. Therefore S/B ratio and significance are not shown for various $p_{T,\text{comb}}$, like is done in Figure 21.

Although the PYTHIA events show the W boson peak quite clearly in Figure 22, the JEWEL events do it even better. There is less background visible, especially for the lower invariant mass region. From Figure 23 it becomes clear that JEWEL, besides making the W boson more distinct, also describes the W boson better. The mean of the W boson mass

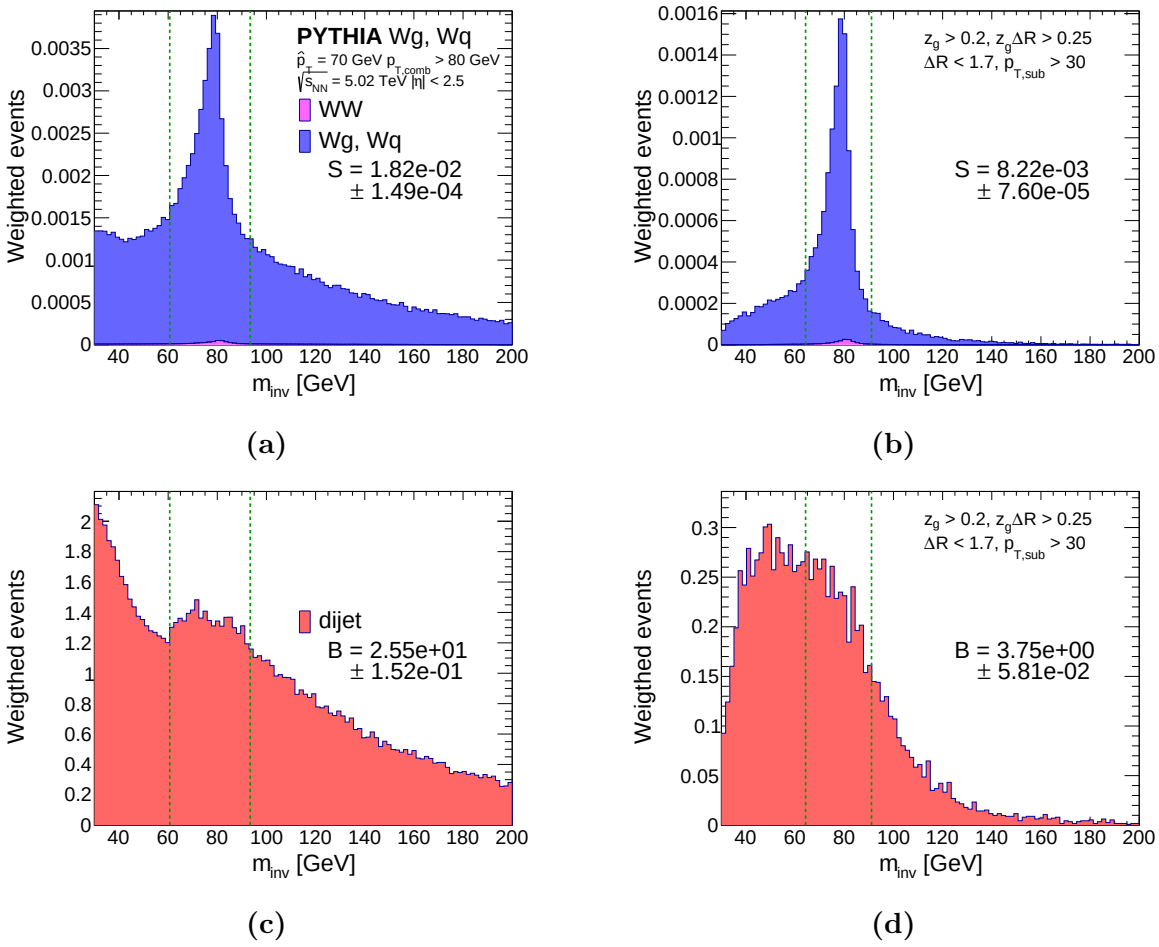

Figure 20: Mass distributions of the signal (Top) and dijet (Bottom) events, weighted by their cross sections (Equation 14), with no cuts (Left) and with the established cuts (Right) $p_{T,\text{sub}} > 30$ GeV, $z > 0.2$, $z\Delta R > 0.25$ and $\Delta R < 1.7$. The green lines indicate the W boson invariant mass region of the Gaussian ($\pm 3\sigma$) and is for clarity also shown in the dijet graphs. A lot of dijet background is cut away when the established cuts are applied, and the sum of the bins within the Gaussian region, so B, divides itself almost seven times when comparing the uncut and established cut dijet events. The peak of the signal events stays very distinct and most of the background in the signal events is cut away. The S/B ratio and significance are shown in Table 3.

Table 3: The S/B ratio and significance $S/\sqrt{S+B}$ for the discussed events, with and without the established cuts $p_{T,\text{sub}} > 30$ GeV, $z > 0.2$, $z\Delta R > 0.25$ and $\Delta R < 1.7$ applied and a reference to the Figure where their mass distribution is depicted. The upper row has dijet events as the background B while the bottom rows have the events within the polynomial background fit as background B. Therefore the S/B ratio and significance can not be compared between these events, the background B is physically something else.

S events	B events	generator	established cuts	S/B ratio	significance	Figure
WW, Wg, Wq Gaussian	dijet	PYTHIA	N	$(0.714\pm 0.00722) \times 10^{-3}$	$(3.61\pm 0.159) \times 10^{-3}$	20a, 20c
			Y	$(2.19\pm 0.0340) \times 10^{-3}$	$(4.24\pm 0.0991) \times 10^{-3}$	20b, 20d
Wg, Wq Gaussian	Wg, Wq Polynomial	PYTHIA	N	0.731 ± 0.963	0.272 ± 0.0670	22a
			Y	3.11 ± 3.69	0.622 ± 0.0747	22b
		JEWEL	N	3.72 ± 11.8	0.540 ± 0.124	22a
			Y	18.4 ± 94.6	0.814 ± 0.930	22b

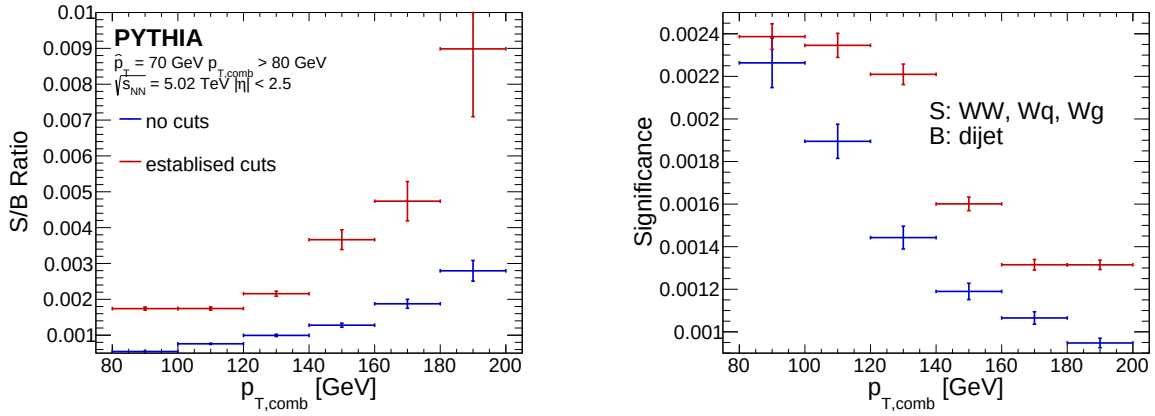

(a) **(b)**

Figure 21: S/B ratio and significance of the W bosons events as signal and dijet event as background, with no cuts and the established cuts $p_{T,\text{sub}} > 30$ GeV, $z > 0.2$, $z\Delta R > 0.25$ and $\Delta R < 1.7$. Both the S/B ratio and significance are higher with the established cuts applied. The S/B ratio increases for higher $p_{T,\text{comb}}$ while the significance decreases. The increasing difference between the S/B ratio when no cuts or the established cuts are applied indicates that the established cuts really focus on W bosons and cut away the background.

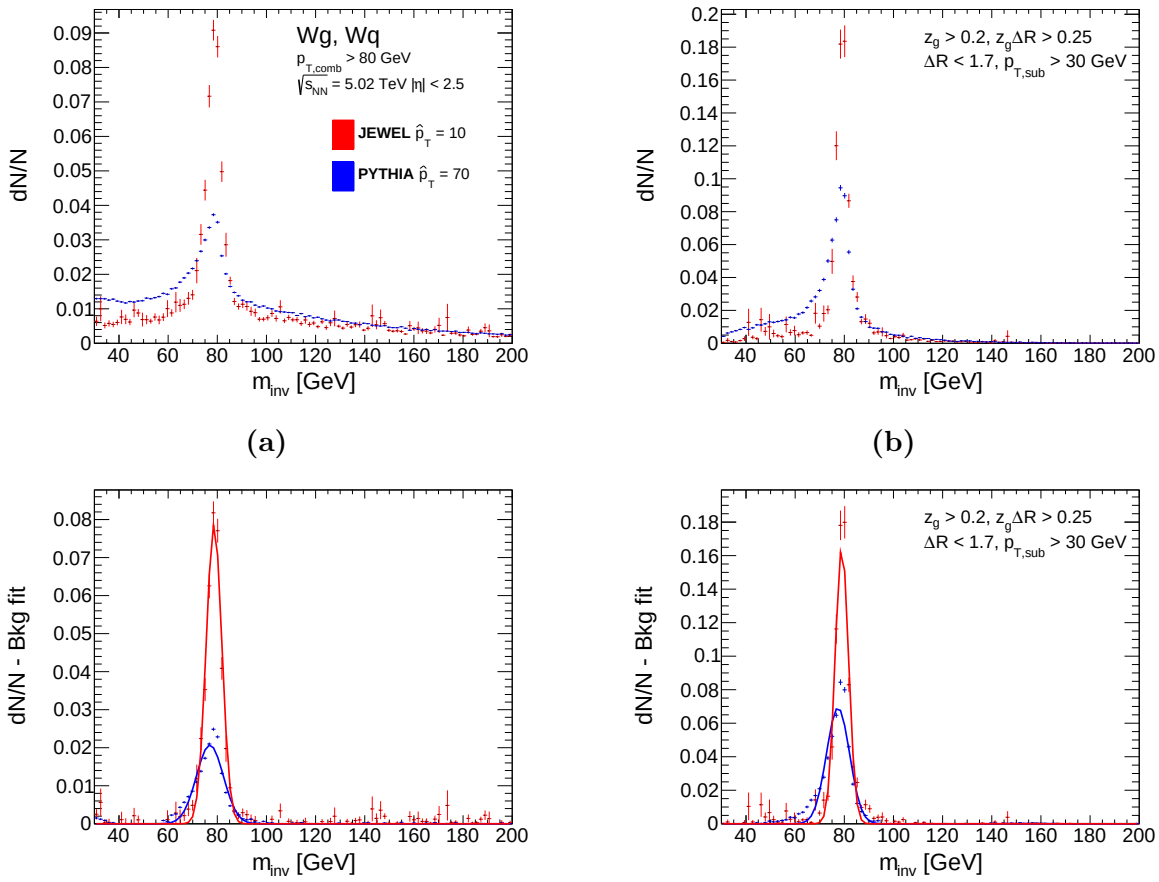

Figure 22: (Top) Total mass distributions of PYTHIA and JEWEL Wg Wq events with no cuts (Left) and with the established cuts (Right) $p_{T,\text{sub}} > 30$ GeV, $z > 0.2$, $z\Delta R > 0.25$ and $\Delta R < 1.7$. (Bottom) The polynomial background fit subtracted from the total mass distribution. The difference of $\hat{p}_T$ between PYTHIA and JEWEL is taken into account with the minimal cut of $p_{T,\text{comb}} > 80$ GeV. The JEWEL W boson peak is way sharper and higher, while the PYTHIA events have more combinatorial background. When the established cuts are applied, this effect is less but still very present.

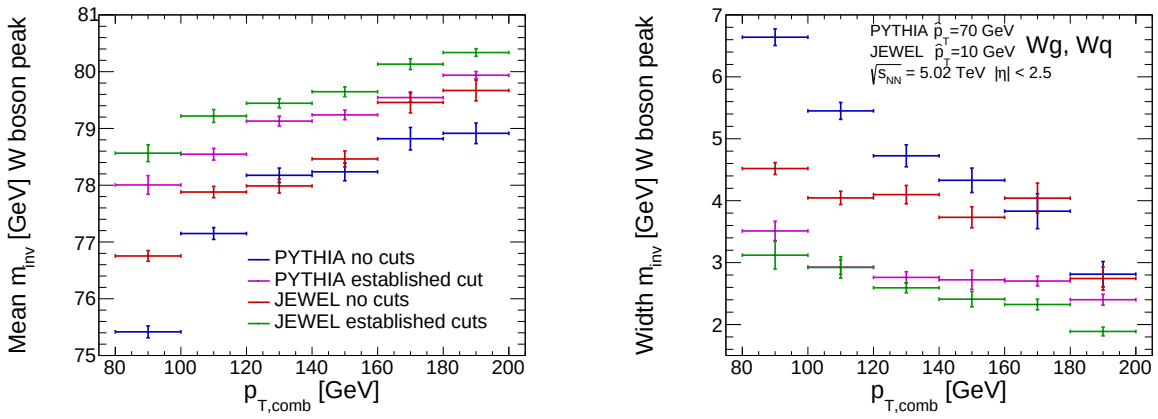

Figure 23: Mean and width of the Gaussian that described the W boson mass for various $p_{T,\text{comb}}$. The W boson mass of 80.376 ± 0.033 GeV gets better described and the width is smaller at higher $p_{T,\text{comb}}$. Applying the established cuts $p_{T,\text{sub}} > 30$ GeV, $z > 0.2$, $z\Delta R > 0.25$ and $\Delta R < 1.7$ does a better job than applying no cuts, both for PYTHIA and JEWEL.

peak is always closer to the true value and the width is always smaller. When the established cuts are applied, both JEWEL and PYTHIA describe the W boson mass peak better than with no cuts applied.

6 Conclusion

The delay of the W boson production in the QGP can teach us about the time evolution of the plasma. To identify W bosons in pp collisions, their jet characteristics are studied in comparison with dijets. We found that a minimal cut on $p_{T,\text{sub}}$, z and $z\Delta R$ and a maximal cut on ΔR have a positive result on the distinctiveness of W bosons in pp collisions. We also found that no minimal cuts should be applied on m_{sub}.

Applying the established cuts, which are $p_{T,\text{sub}} > 30$ GeV, $z > 0.2$, $z\Delta R > 0.25$ and $\Delta R < 1.7$, together improved their performance better than when they are applied alone. So different W bosons characteristics are correlated and can be used to describe W bosons. With this description of them, they can be distinguished in dijet events. The S/B ratio and significance that was found is still far too low to distinguish W bosons in dijet events. Therefore it will not be possible to distinguish them in real measurements, for that we need both the S/B ratio and significance to have a minimal value of three. So although the established cuts do a good job by increasing the S/B ratio and significance, they do not enough to be satisfying.

The established cuts are optimised for cutting away underlying events in the form of dijet events. But the established cuts also have proven to do a good job by cutting away combinatorial background. The W boson combinatorial background, which is under the Gaussian in Figure 22, decreases a lot more than the pure W boson signal when the cuts are applied. This proves once again that the established cuts do a good job by focusing the data op W bosons. The established cuts also describe the W bosons better. When the established

cuts are applied, the W boson mass peak lies closer to the true value, as depicted in Figure 23.

In JEWEL is jet quenching taken into account and in PYTHIA it is not. If jets are quenched, they have lost energy to the QGP, which would result in a smaller invariant mass peak. It could be expected that the W boson peak would also be wider because of the energy loss to the plasma. The opposite is visible in Figures 22 and 23. The W boson mass peak in JEWEL is higher, has a smaller width and lies closer to the true value. This could indicate that jet quenching has a positive influence on the distinctiveness of W bosons.

7 Discussion & Outlook

In Section 4.2, the best background fit of WW events is, with the use pull distributions, determined to be a fourth order polynomial. During the rest of the analysis, this fourth order polynomial is used as the background fit for all the events and cuts. The assumption that all background is adequately described by a fourth order polynomial is premature. The background changes when cuts are applied or other events are generated, so a fourth order polynomial can be insufficient to fit the background to. On the other hand, a fourth order polynomial already has four degrees of freedom and can take on many shapes. So although it may have happened that another fit function could be used better for specific cuts and events, the used fourth order polynomial often did a sufficient job.

At the end of the Theory, in Section 2.7, are the discussed characteristics listed in Table 1. The number of characteristics and regions of them are narrowed down by studying the resolution, which is the width of the response ratio of the signal events and constituent subtracted events. By narrowing down based on results from the response ratio we assume that a comparison between the signal and constituent subtracted events is similar to a comparison between the signal and dijet events. This is not very physically. Pure W boson signal events do not occur in real measurement because the smallest collisions possible are pp collisions, and not parton-parton collision. The comparison between pure W boson signal events and constituent subtracted W boson events can form a stepping stone to the comparison between W boson events and dijet events but will not always be accurate.

An instance where this generalisation goes wrong is the characteristic ΔR. The resolution of the response ratio is not aligning with the behaviour of the S/B ratio and significance. The behaviour of the S/B ratio when m_{sub} is varied does not align with what we would expect from the resolution. The odd behaviour of the response ratio of $p_{T,\text{lead}}$ has also not been investigated. These three oddities are examples that could be further examined.

In further research, the number and kind of established cuts could also be extended. Mainly based on the response ratio's, three minimal cuts and one maximal cut are established. Cuts on more characteristics and regions within characteristics, instead of minimal or maximal cuts, could improve the S/B ratio and significance. The use of machine learning could be a great help when doing this. When determining more and sharper cuts, more data will be lost. Increasing the number of events will solve this and will also increase the significance, which was very low in this study.

The fact the W boson mass peak from JEWEL events was sharper, smaller and closer

to the true value is surprising. The reasoning that this indicates that jet quenching has a positive influence on the distinctiveness of W bosons could be naive. A further investigation of the theoretical effects of jet quenching and the differences between PYTHIA and JEWEL is needed to draw any firm conclusion.

Lastly, all the discussed events were generated PYTHIA or JEWEL. These stay event generators en describe only partly the reality. In further research, the established cuts could be applied on experimental measurements.

References

[1] C. Manuel, *The Stopping Power of Hot Nuclear Matter* (2014).

[2] U. W. Heinz, *Concepts of heavy-ion physics* (2004), hep-ph/0407360.

[3] CERN, *The Large Hadron Collider*, https://home.cern/science/accelerators/large-hadron-collider (2020).

[4] M. Connors, C. Nattrass, R. Reed, and S. Salur, Reviews of Modern Physics **90** (2018), ISSN 1539-0756, URL http://dx.doi.org/10.1103/RevModPhys.90.025005.

[5] D. d' Enterria, Landolt-Börnstein - Group I Elementary Particles, Nuclei and Atoms p. 471–520 (2010), ISSN 1616-9522, URL http://dx.doi.org/10.1007/978-3-642-01539-7_16.

[6] L. Apolinário, J. G. Milhano, G. P. Salam, and C. A. Salgado, Physical Review Letters **120** (2018), ISSN 1079-7114, URL http://dx.doi.org/10.1103/PhysRevLett.120.232301.

[7] A. Ali and G. Kramer, The European Physical Journal H **36**, 245–326 (2011), ISSN 2102-6467, URL http://dx.doi.org/10.1140/epjh/e2011-10047-1.

[8] K. Aamodt et al. (ALICE), JINST **3**, S08002 (2008).

[9] CERN, International Journal of Modern Physics A **29**, 1430044 (2014), ISSN 1793-656X, URL http://dx.doi.org/10.1142/S0217751X14300440.

[10] B. Abelev, J. Adam, D. Adamová, M. M. Aggarwal, G. Aglieri Rinella, M. Agnello, A. Agostinelli, N. Agrawal, Z. Ahammed, N. Ahmad, et al. (ALICE Collaboration), Tech. Rep. CERN-LHCC-2013-024. ALICE-TDR-017, CERN (2013), URL https://cds.cern.ch/record/1625842.

[11] CERN, *More details on the ALICE ITS*, http://alice.web.cern.ch/detectors/more-details-alice-its.

[12] G. Dellacasa et al. (ALICE) (2000).

[13] CERN, *More details on the ALICE TPC*, http://alice.web.cern.ch/detectors/more-details-alice-tpc.

[14] B. R. Martin, *Nuclear and Particle Physics* (John Wiley & Sons Ltd., 2009).

[15] T. Hülsing, Ph.D. thesis, Johannes Gutenberg-Universität Mainz (2014), presented 22 Jan 2015, URL https://cds.cern.ch/record/1983158.

[16] A. Majumder, Physical Review D **85** (2012), ISSN 1550-2368, URL http://dx.doi.org/10.1103/PhysRevD.85.014023.

[17] D. S. Cerci (CMS), *Soft and Hard QCD Processes in CMS* (2017).

[18] D. d'Enterria and B. Betz, *High-pT Hadron Suppression and Jet Quenching* (Lecture Notes in Physics, 2009), vol. 785, pp. 285–339.

[19] M. Schott and M. Dunford, The European Physical Journal C **74** (2014), ISSN 1434-6052, URL http://dx.doi.org/10.1140/epjc/s10052-014-2916-1.

[20] G. Abbiendi, K. Ackerstaff, C. Ainsley, P. Akesson, G. Alexander, J. Allison, K. Anderson, S. Arcelli, S. Asai, S. Ashby, et al. (OPAL Collaboration), Phys. Lett. B **493**, 249 (2000), 22 pages, 5 figures, submitted to Phys. Lett. B Report-no: CERN-EP-2000-101, URL https://cds.cern.ch/record/457402.

[21] S. Marzani, G. Soyez, and M. Spannowsky, Lecture Notes in Physics (2019), ISSN 1616-6361, URL http://dx.doi.org/10.1007/978-3-030-15709-8.

[22] A. J. Larkoski, J. Thaler, and W. J. Waalewijn, Journal of High Energy Physics **2014** (2014), ISSN 1029-8479, URL http://dx.doi.org/10.1007/JHEP11(2014)129.

[23] M. Cacciari, G. P. Salam, and G. Soyez, The European Physical Journal C **72** (2012), ISSN 1434-6052, URL http://dx.doi.org/10.1140/epjc/s10052-012-1896-2.

[24] P. Schieferdecker, *Jet algorithms*, https://twiki.cern.ch/twiki/bin/viewfile/Sandbox/Lecture?rev=1;filename=Philipp_Schieferdeckers_Lecture.pdf.

[25] K. Kauder, Nuclear Physics A **967**, 516–519 (2017), ISSN 0375-9474, URL http://dx.doi.org/10.1016/j.nuclphysa.2017.07.004.

[26] M. Tanabashi, K. Hagiwara, K. Hikasa, K. Nakamura, Y. Sumino, F. Takahashi, J. Tanaka, K. Agashe, G. Aielli, C. Amsler, et al. (Particle Data Group), Phys. Rev. D **98**, 030001 (2018), URL https://link.aps.org/doi/10.1103/PhysRevD.98.030001.

[27] Lund University, *Pythia 8*, http://home.thep.lu.se/~torbjorn/pythia81html/Welcome.html.

[28] HEPForge, *JEWEL*, https://jewel.hepforge.org/.

[29] M. Caccoaro, G. P. Salam, and G. Soyes, *Fastjet*, http://fastjet.fr/.

[30] CERN, *ROOT - A data analysis framework*, https://root.cern.ch/.

[31] T. M. Karbach and M. Schlupp, *Constraints on yield parameters in extended maximum likelihood fits* (2012), 1210.7141.

[32] M. Moshinsky, J. Patera, R. T. Sharp, and P. Winternitz, Annals of Physics **95**, 129 (1975).

[33] CERNBox, *Samples — Thermal — Mult45000*, https://cernbox.cern.ch/index.php/s/kRy9M7NC9iilE9Z?path=%2Fsamples%2Fthermal%2FMult4500.

[34] I. Dremin and J. Gary, Physics Reports **349**, 301–393 (2001), ISSN 0370-1573, URL http://dx.doi.org/10.1016/S0370-1573(00)00117-4.

[35] S. Acharya, D. Adamová, M. Aggarwal, G. Aglieri Rinella, M. Agnello, N. Agrawal, Z. Ahammed, N. Ahmad, S. Ahn, S. Aiola, et al., Physics Letters B **776**, 249–264 (2018), ISSN 0370-2693, URL http://dx.doi.org/10.1016/j.physletb.2017.11.044.

A Appendix

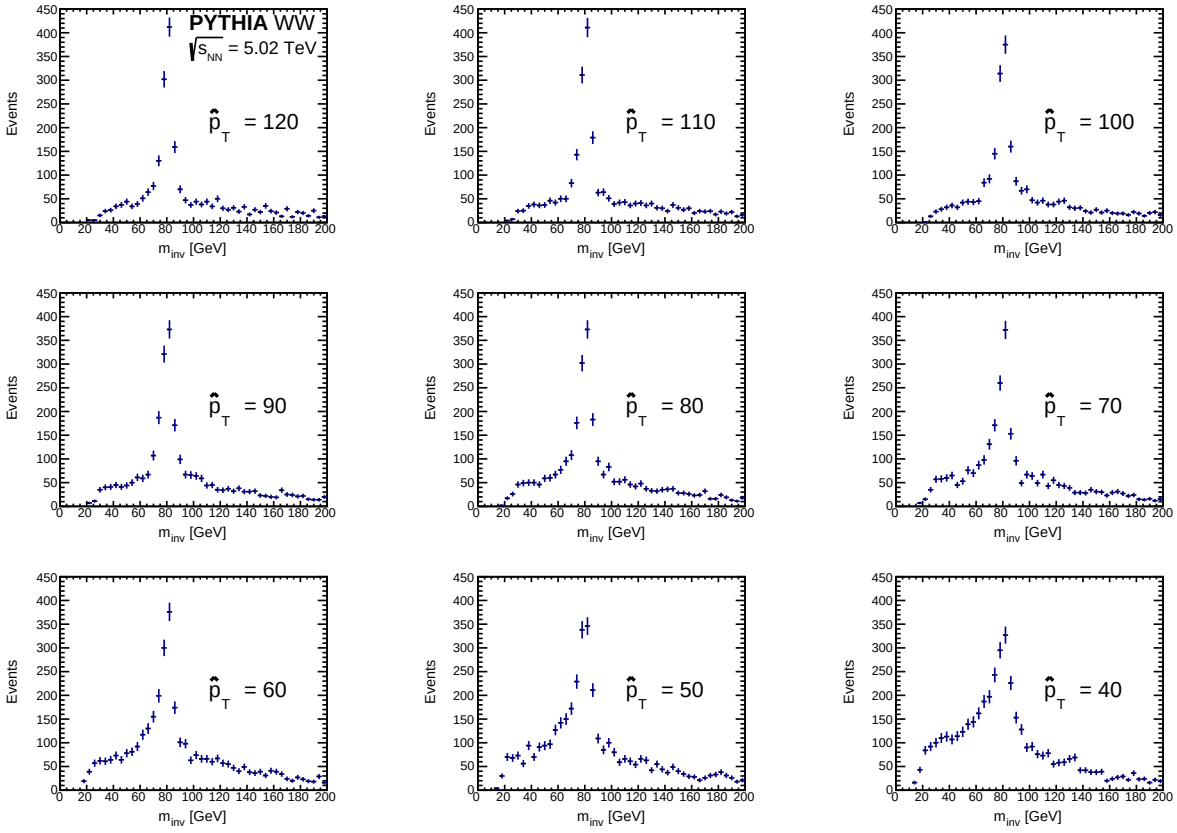

Figure A.1: Invariant mass distribution of WW events for various $\hat{p}_T$. The higher the $\hat{p}_T$, the sharper and higher the peak is around the W boson mass. For lower $\hat{p}_T$, the mass get less distinct which makes distinguishing W bosons harder. At higher $\hat{p}_T$ there are fewer events overall which can result in too few events to have enough statistics. Se there is a trade off between enough statistics and enough distinctness of W bosons when varying $\hat{p}_T$.

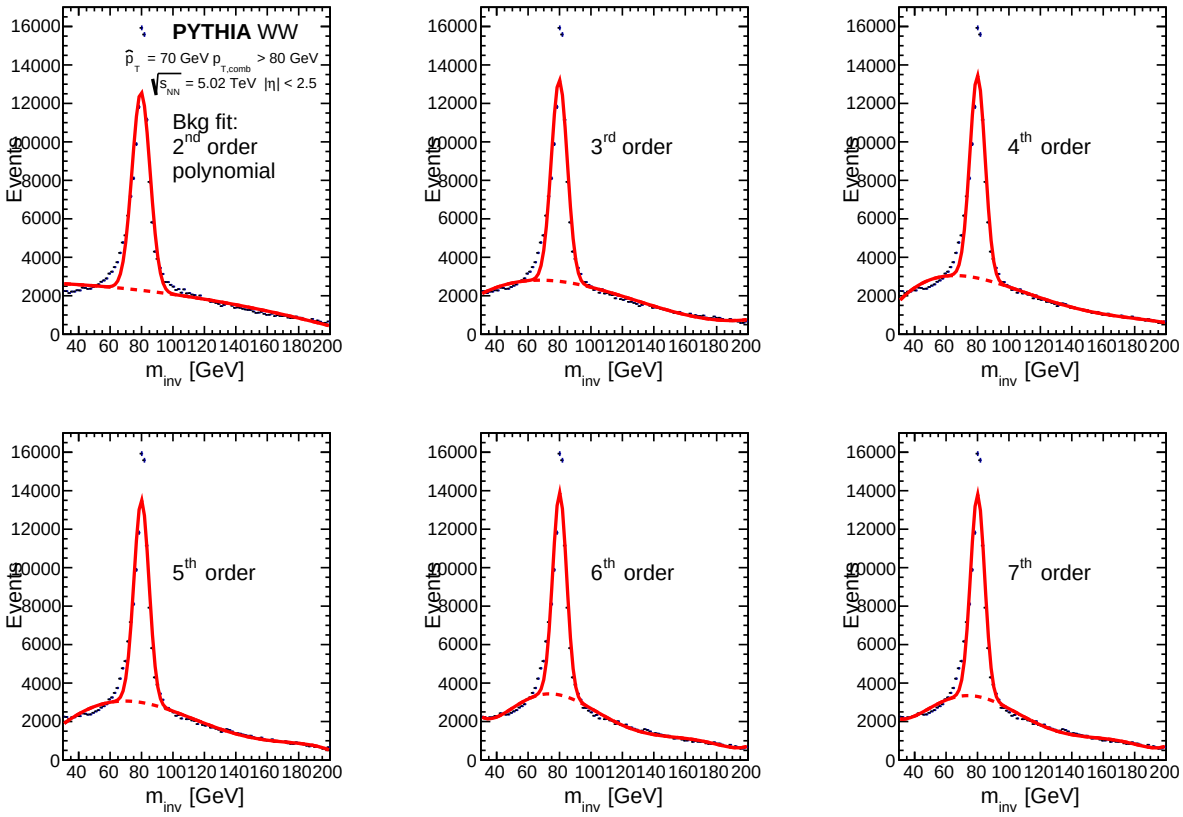

Figure A.2: Various fits for the same mass distribution of WW events. The fitted function is a Gaussian plus a polynomial. The order of polynomial is varied between two and seven. A fit with a second order polynomial has clearly some flaws close to the Gaussian and for lower invariant masses. The higher order polynomials do not differ much and do a similar, good job of fitting the invariant mass distribution.

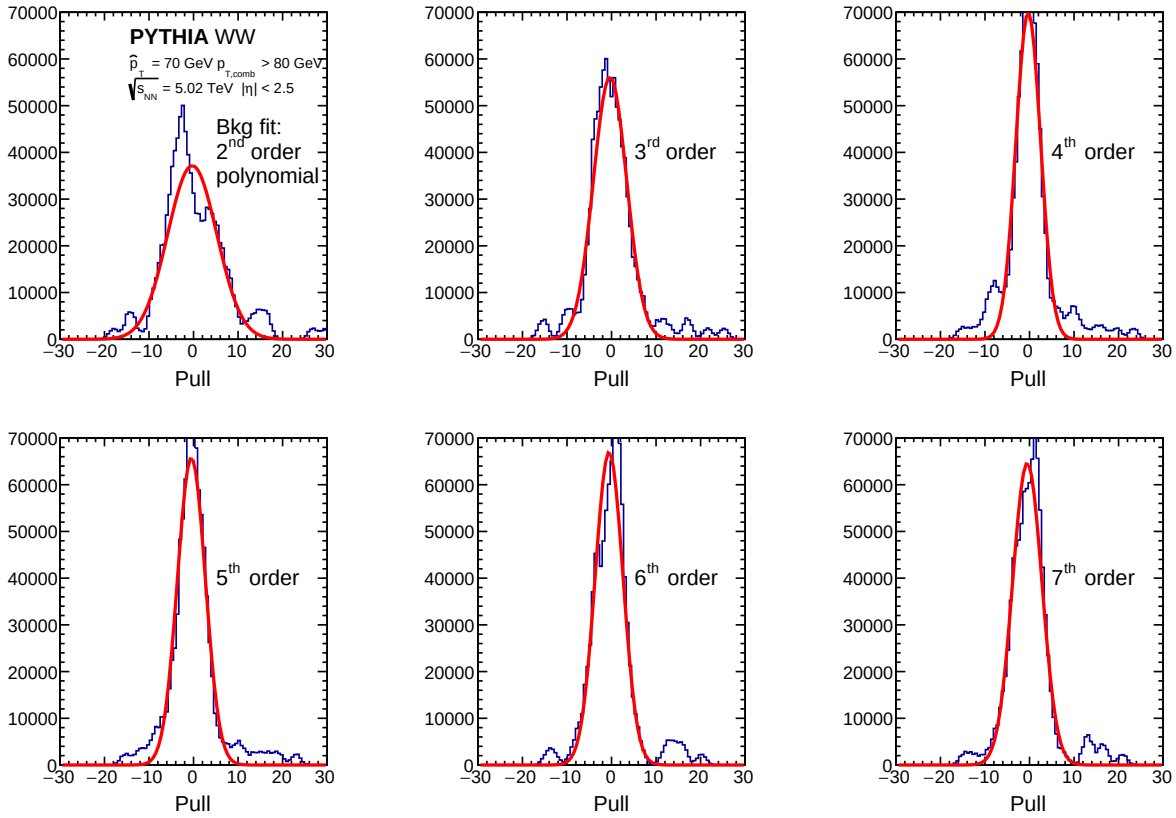

Figure A.3: Fits of the pull distributions of the various fits for the same mass distribution of WW events (Figure A.2. The pull distribution is fitted by a Gaussian. The mean and width of that Gaussian are shown in Figure 7. The pull distributions of the second and third order polynomial are wider that the other order polynomials. All have some flaws in the form of small peaks after the Gaussian has died out, where the pull is between 10 and 20.

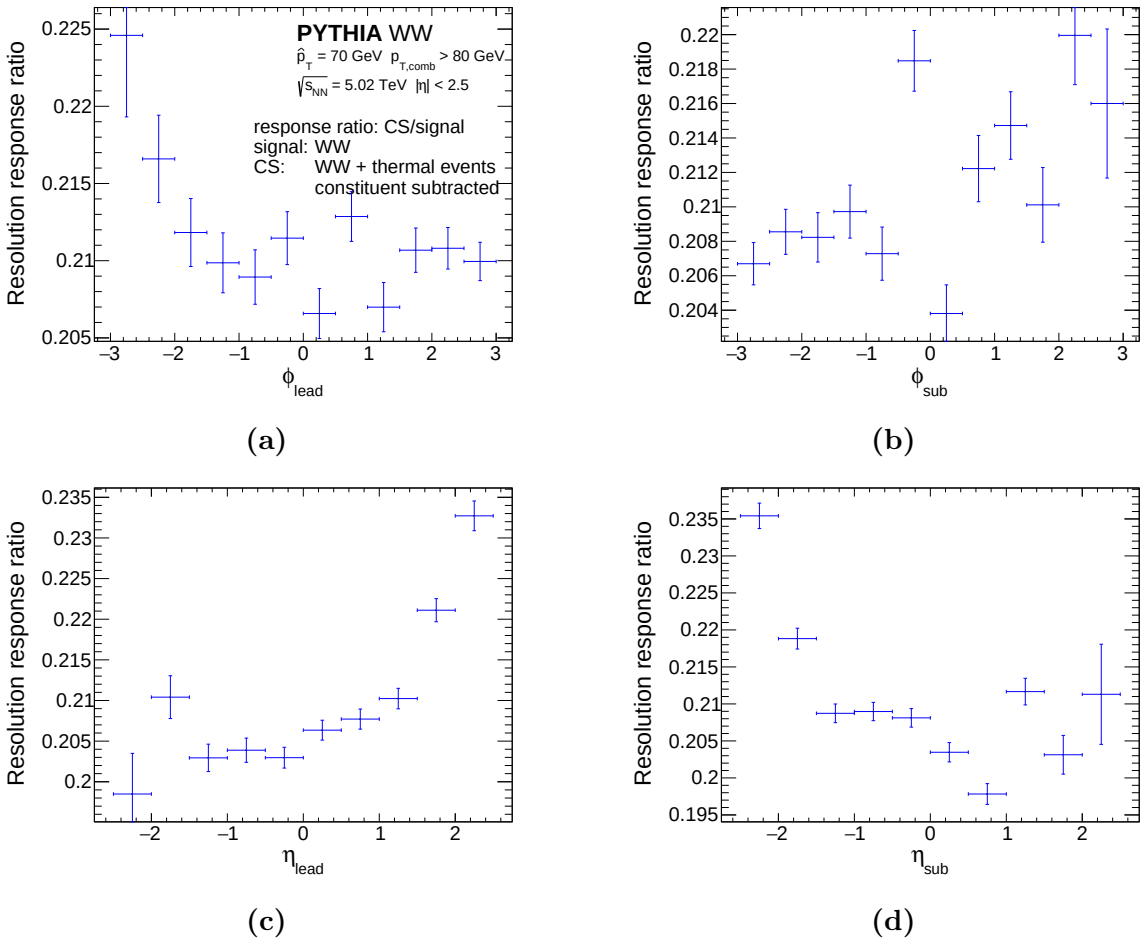

Figure A.4: Resolution of η and ϕ for both the leading and subleading jets. The resolution of all four does not show a distinct dependence on one of the jet characterisations. This is expected, since it should not matter in which direction the jets propagate.

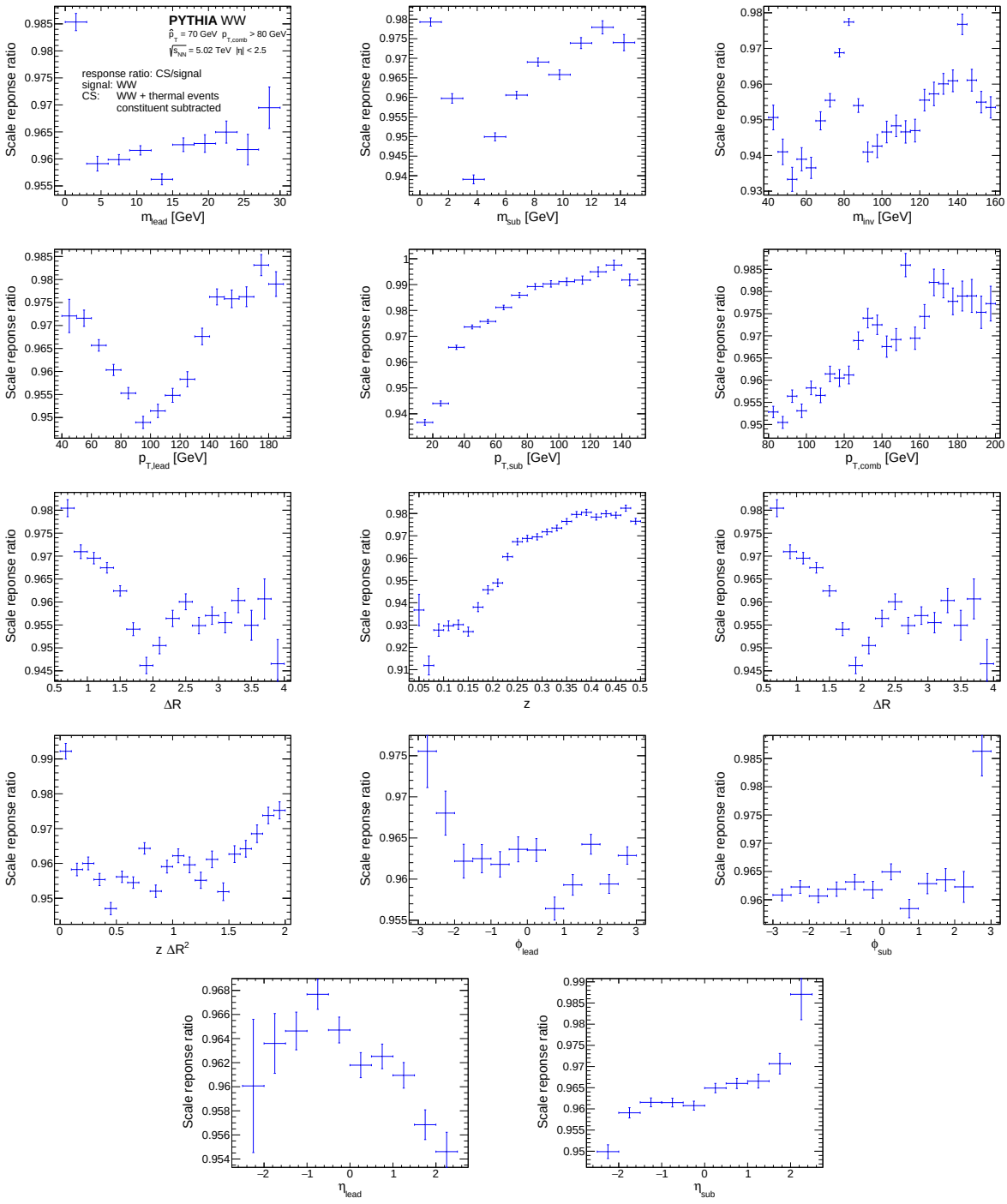

Figure A.5: Scale when varying jet characterisations. The scale is the mean of the response ratio of the signal and constituent subtracted events. The response ratio's are close enough to use. Further insides are given by the resolution, the width of the response ratio's.

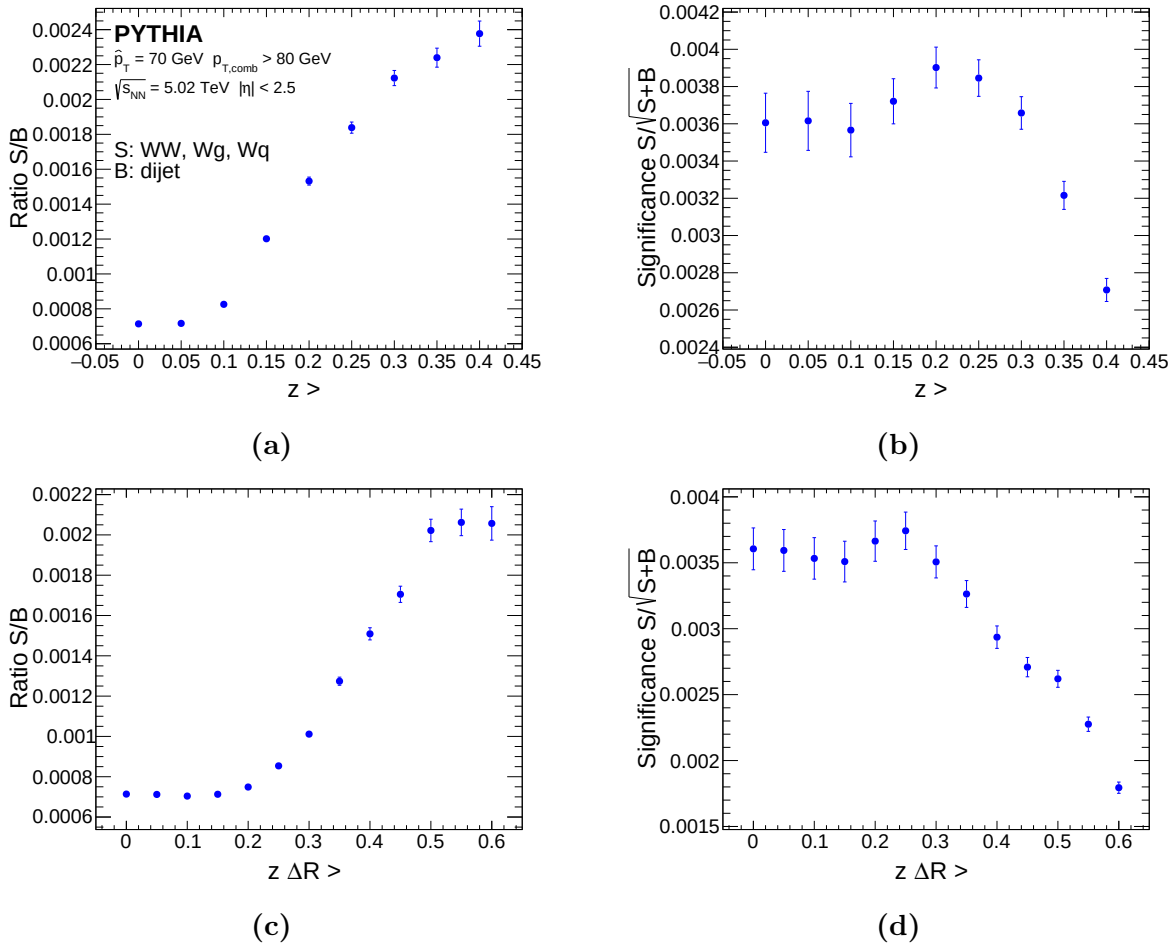

Figure A.6: Ratio and significance of the invariant mass distribution with minimal cuts on z and $z\Delta R$. Both show a similar behaviour as $p_{T,\text{sub}}$ in Figure 15. The S/B ratio is always increasing for higher minimal cuts. The significance is initially stable but drops after a small peak for higher minimal cuts. So there is a trade off between the S/B ratio and significance.